nature cardiovascular research

Article

https://doi.org/10.1038/s44161-024-00546-5

RNF20-mediated transcriptional pausing and VEGFA splicing orchestrate vessel growth

Received: 6 April 2023

Accepted: 29 August 2024

Published online: 25 September 2024

Check for updates

Nalan Tetik-Elsherbiny[1], Adel Elsherbiny[1], Aadhyaa Setya[1], Johannes Gahn[2], Yongqin Tang[1], Purnima Gupta[2], Yanliang Dou[1], Heike Serke[1,3], Thomas Wieland[3,4], Alexandre Dubrac[5], Joerg Heineke[3,6], Michael Potente[3,7,8,9], Julio Cordero[1,3] ✉, Roxana Ola[2,3] ✉ & Gergana Dobreva[1,3,9] ✉

Signal-responsive gene expression is essential for vascular development, yet the mechanisms integrating signaling inputs with transcriptional activities are largely unknown. Here we show that RNF20, the primary E3 ubiquitin ligase for histone H2B, plays a multifaceted role in sprouting angiogenesis. RNF20 mediates RNA polymerase (Pol II) promoter-proximal pausing at genes highly paused in endothelial cells, involved in VEGFA signaling, stress response, cell cycle control and mRNA splicing. It also orchestrates large-scale mRNA processing events that alter the bioavailability and function of critical pro-angiogenic factors, such as VEGFA. Mechanistically, RNF20 restricts ERG-dependent Pol II pause release at highly paused genes while binding to Notch1 to promote H2B monoubiquitination at Notch target genes and Notch-dependent gene expression. This balance is crucial, as loss of *Rnf20* leads to uncontrolled tip cell specification. Our findings highlight the pivotal role of RNF20 in regulating VEGF–Notch signaling circuits during vessel growth, underscoring its potential for therapeutic modulation of angiogenesis.

Formation of blood vessels requires precise coordination of cellular and molecular events guided by signaling cues. Highly mitogenic and plastic venous endothelial cells (ECs) serve as the primary source for angiogenic expansion, a process orchestrated by vascular endothelial growth factor (VEGF) and Notch signaling gradients[1–11]. Venous ECs migrate against the flow in a process known as reverse migration, and the ECs at the leading edge of the newly formed sprout, exposed to the highest VEGFA levels, give rise to tip cells[3,6,7,10–12]. VEGF binding to the pro-angiogenic receptor VEGFR2 in tip cells results in activation of tip cell-enriched genes, such as VEGFR3 and the Notch ligand delta-like 4 (DLL4), among others. Increased DLL4 in tip cells activates Notch signaling in the adjacent stalk ECs, thereby limiting VEGF signaling and sprouting behavior in these stalk cells[1–11]. Tip cells with high Notch activity become pre-specified for an arterial fate and will subsequently contribute to arteries through the same reverse migration process[7]. Signal-responsive gene expression is essential for the tight control of cell state transitions during vessel development, yet the mechanisms allowing the integration of signaling inputs and transcriptional activities during vascular growth and patterning are largely unknown.

In the past decade, it has become clear that signal-dependent transcription is primarily regulated after transcription initiation, through the pausing and release of promoter-proximal RNA polymerase (Pol II)[13–15]. After recruitment to the promoter by transcription factors (TFs) and transcription initiation, Pol II often pauses after the synthesis

A full list of affiliations appears at the end of the paper. ✉e-mail: julio.cordero@medma.uni-heidelberg.de; roxana.ola@medma.uni-heidelberg.de; gergana.dobreva@medma.uni-heidelberg.de

of a short nascent RNA (~20–60 nucleotides (nt)). Pol II stalls after the binding of two pause-inducing factors, NELF and DSIF, and remains in a paused state until additional signals promote productive elongation. Upon activation by different cues, positive elongation factors P-TEFb and TFIIS induce pause release[16]. Paused Pol II is instrumental for rapid and synchronous gene induction by different signaling cues and for ensuring stoichiometric transcripts for genes encoding different subunits of multicomponent protein transcriptional complexes. Environmental (for example, heat shock, hypoxia and inflammation), developmental and differentiation signals have been shown to regulate Pol II pausing and release[14,15]. For example, before HIF1A activation upon hypoxia, its target genes harbor transcriptionally engaged paused Pol II. HIF1A binding and recruitment of the P-TEFb complex results in Pol II pause release for active elongation of HIF1A target genes[17]. Similarly, VEGFA stimulation rapidly induces overall Pol II pause release, primarily at early upregulated genes[18]. Sensing and responding to signals is central to the function of the endothelium; however, the molecular players that regulate these processes are poorly understood.

RNF20, the major E3 ubiquitin ligase responsible for monoubiquitination of histone H2B at lysine 120 (H2BK120ub, H2Bub1)[19–21], plays a key role in transcriptional pausing and elongation by Pol II. On the one hand, RNF20-mediated H2Bub1 facilitates FACT function in promoting transcriptional elongation by destabilizing nucleosomes[21]. Conversely, RNF20 impedes the recruitment of TFIIS, necessary for releasing Pol II into active elongation at genes that promote tumorigenesis, thus repressing pro-oncogenic transcriptional programs[22]. Interestingly, mutations in the *RNF20* gene have been associated with cardiovascular malformations in human patients[23], and a recent study revealed that RNF20-regulated EC-born signals orchestrate neural precursor cell fate during embryogenesis[24]. Despite its important molecular functions and the intriguing findings mentioned above, the role of RNF20 in ECs remains largely unexplored.

Results

The E3 ubiquitin ligase RNF20 orchestrates sprouting angiogenesis

Analysis of single-cell RNA sequencing (RNA-seq) datasets of ECs from postnatal day 6 (P6) and P10 retinas[25] revealed temporal and spatial expression dynamics of *Rnf20* in ECs. *Rnf20* levels were lowest in venous and significantly higher in tip ECs, with highest levels in arterial ECs at early postnatal stages (P6) (Fig. 1a and Extended Data Fig. 1a). At P10, *Rnf20* levels were generally lower when compared to P6 (Extended Data Fig. 1a). This differential expression pattern suggested a potential role for RNF20 in regulating tip and/or arterial identity of ECs.

To understand the function of RNF20 in vessel growth, we generated tamoxifen-inducible EC-specific *Rnf20* knockout mice by crossing *Rnf20 fl/fl* to *Pdgfb-CreERT2* mice (hereafter referred to as *Rnf20*$^{iEC\text{-}KO}$ mice) (Extended Data Fig. 1b) and studied the impact of EC *Rnf20* deletion on postnatal retinal angiogenesis. 4-hydroxy-tamoxifen (4-OHT) was administered to *Rnf20*$^{iEC\text{-}KO}$ and Cre-negative littermates (controls) from P1 to P4, and mice were analyzed at P7 (Fig. 1b). Gene deletion in the ECs was confirmed by real-time quantitative polymerase chain reaction (RT–PCR) and western blot (WB) analysis of ECs purified from P7 lungs (Extended Data Fig. 1c,d). Compared to controls, *Rnf20*$^{iEC\text{-}KO}$ mutant mice showed no differences in gross appearance or body weight (Extended Data Fig. 1e); however, endothelial *Rnf20* loss led to a significant decrease in the retinal vessel outgrowth (Fig. 1c,d) accompanied by shortening of arteries and veins and an extended vascular front (Fig. 1e,f and Extended Data Fig. 1f). Endothelial sprouts at the extended vascular front displayed thinner morphology and a smaller lumen, indicated by CD31 and ICAM2 co-immunostaining (Fig. 1g). Mutant ECs also had more and longer filopodia at the sprouting front (Fig. 1h–j). As these cellular characteristics resemble tip-like ECs, we next immunostained P7 retinas for the VEGF-regulated tip cell marker ESM1 (ref. 26) (Fig. 1k,l and Extended Data Fig. 1g). This analysis revealed a striking increase in ESM1-positive ECs, suggesting that *Rnf20* deficiency promotes the acquisition of a tip cell-like phenotype.

To study if the increased tip cell number is due to an increased EC proliferation, we labeled endothelial nuclei with antibodies against the TF ERG (marking endothelial nuclei) and CD31 (marking endothelial junctions). Quantification of the ERG-positive nuclei revealed a decreased number of ECs per vascular area (Fig. 1m,n). In addition, endothelial 5-ethynyl-2′-deoxyuridine (EdU) incorporation was also decreased in *Rnf20*$^{iEC\text{-}KO}$ ECs (Fig. 1o,p), suggesting that RNF20 is important for EC proliferation and that the increased tip cell number is independent of EC proliferation. Previous studies showed that CreERT toxicity might affect retinal angiogenesis and, thus, can confound interpretation of the effect of specific gene deletion[27]. Analysis of Pdgfb-CreERT2-positive versus Pdgfb-CreERT2-negative P7 retinas after the same 4-OHT administration regimen, however, did not find significant differences in radial length, vascular front, the length of arteries and veins or ESM1 staining (Extended Data Fig. 1h–k).

Timecourse imaging studies in zebrafish and mice showed that venous ECs polarize and migrate against the blood flow (reverse migration) to give rise to tip cells that are later recruited into arteries[3,7,11,12]. To assess if the increased tip cell number and the shortened arteries are due to defective polarization, we labeled control and *Rnf20*$^{iEC\text{-}KO}$ retinas for the Golgi marker Golph4/GPP130, SOX17 and isolectin B4 (IB4) to visualize the EC orientation (Fig. 1q–s). The relative position of the Golgi and nuclei at the vascular front close to arteries were then quantified (Fig. 1s). We found an increase of cells non-oriented or oriented with flow in *Rnf20*$^{iEC\text{-}KO}$ retinas, suggesting that EC polarization against the expected flow direction was impaired (Fig. 1s). These results suggest that compromised migration against the flow might lead to accumulation of the tip cells upon *Rnf20* loss of function (LOF).

Fig. 1 | RNF20 suppresses tip EC identity. a, Violin plot showing minimum, 25th percentile (Q1), median, 75th percentile (Q3) and maximum *Rnf20* expression levels in venous ($n = 504$), tip ($n = 189$) and arterial ($n = 192$) ECs (left) and dot plot of the expression level and frequency of markers for these different cell populations in P6 and P10 retinas (right)[25]. The *P* values were calculated using a likelihood-ratio test from the FindMarkers function in Seurat (version 4.1.0). **b**, Schematic representation of the experimental setup for the data shown in **c**–**s**. **c**,**d**, Representative confocal images of control ($n = 10$) and *Rnf20*$^{iEC\text{-}KO}$ ($n = 10$) retina at P7 stained with the EC marker PECAM1 (CD31) (**c**) and quantification of the radial length (**d**). **e**,**f**, Overview of retinal vascular plexus of P7 control and *Rnf20*$^{iEC\text{-}KO}$ mice stained with IB4 (**e**) and quantification of the length of the vascular front (**f**); $n = 10$ retinas for each group (**f**). A, artery; V, vein. **g**,**i**, Co-immunostaining of mouse retina at P7 with CD31 and ICAM2 (labeling the vascular lumen) (**g**) or CD31 alone (**i**). **h**, Quantification of filopodia length of control and *Rnf20*$^{iEC\text{-}KO}$ retina ECs at P7; $n = 5$ control and $n = 8$ *Rnf20*$^{iEC\text{-}KO}$ retinas. **j**, Quantification of filopodia number per 100-µm vessel length; $n = 5$ control and $n = 8$ *Rnf20*$^{iEC\text{-}KO}$ retinas. **k**,**l**, Immunostaining for ESM1 (tip cell marker) and CD31 (**k**) and quantification of tip cell numbers (**l**); $n = 5$ control and $n = 8$ *Rnf20*$^{iEC\text{-}KO}$ retinas. **m**,**n**, Immunostaining for ERG (labeling EC nuclei) and CD31 (**m**) and quantification of EC number; $n = 4$ control and $n = 3$ *Rnf20*$^{iEC\text{-}KO}$ retinas (**n**). **o**,**p**, Labeling for EdU and ERG (**o**) and quantification of double-EdU/ERG-positive ECs; $n = 5$ control and $n = 6$ *Rnf20*$^{iEC\text{-}KO}$ retinas (**p**). **q**,**r**, Immunostaining for SOX17 and the Golgi marker Golph4/GPP130 of control and *Rnf20*$^{iEC\text{-}KO}$ retinas (**q**) and schematic drawing representing the Golgi orientation presented in **q** (**r**). **s**, Quantification of EC polarization; $n = 4$ retinas for each group. Figure represents mean ± s.e.m.; statistics were quantified with two-way ANOVA with Sidak's correction. Each dot in **d**, **f**, **h**, **j**, **l**, **n** and **p** represents quantification from different leaflets of the indicated number (*n*) of retinas, each isolated from an individual mouse. Data are represented as mean ± s.e.m.; differences between groups were assessed using an unpaired two-tailed Student's *t*-test. Numeric *P* values are shown within the figure panels. Ctr, control.

https://doi.org/10.1038/s44161-024-00546-5

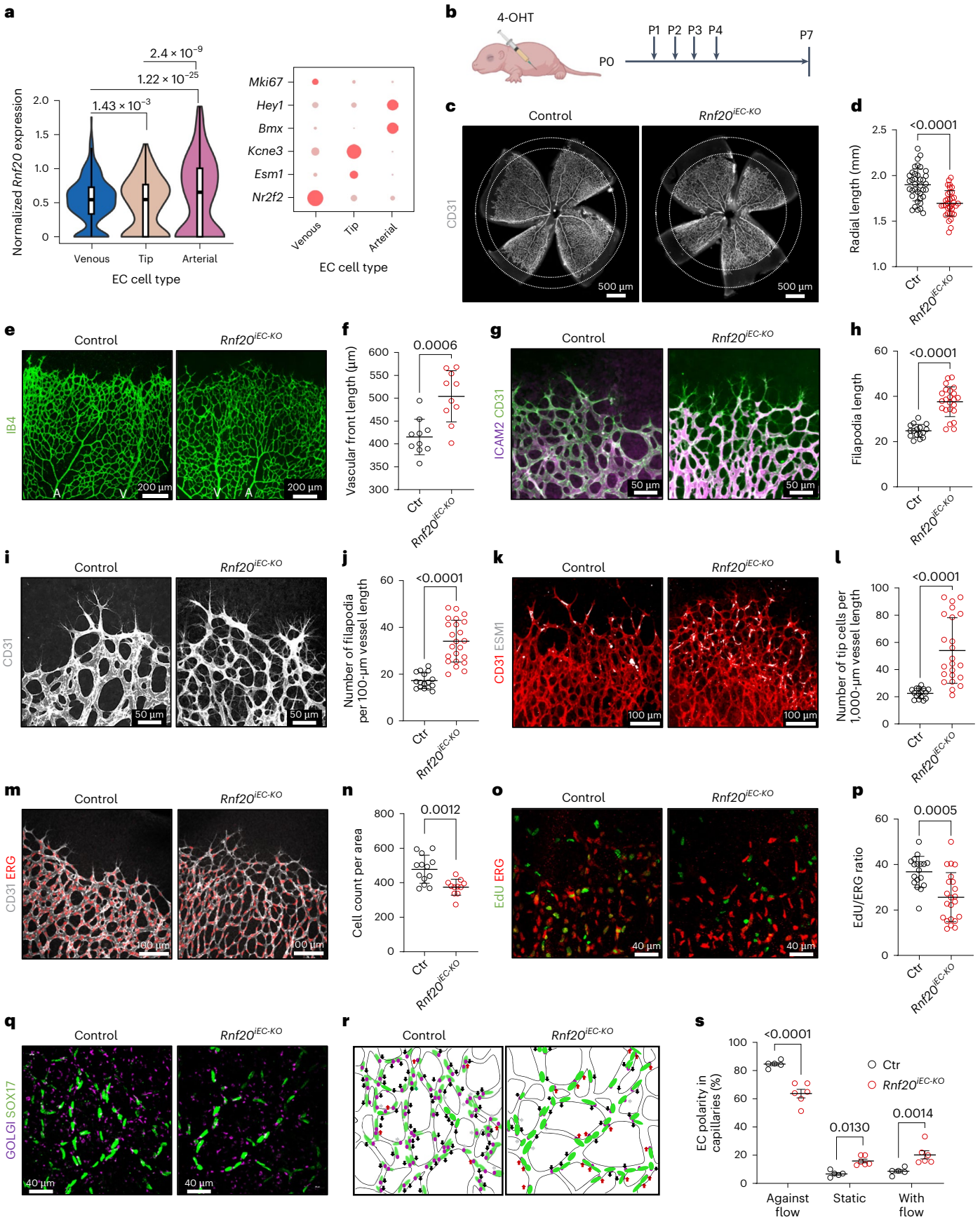

https://doi.org/10.1038/s44161-024-00546-5

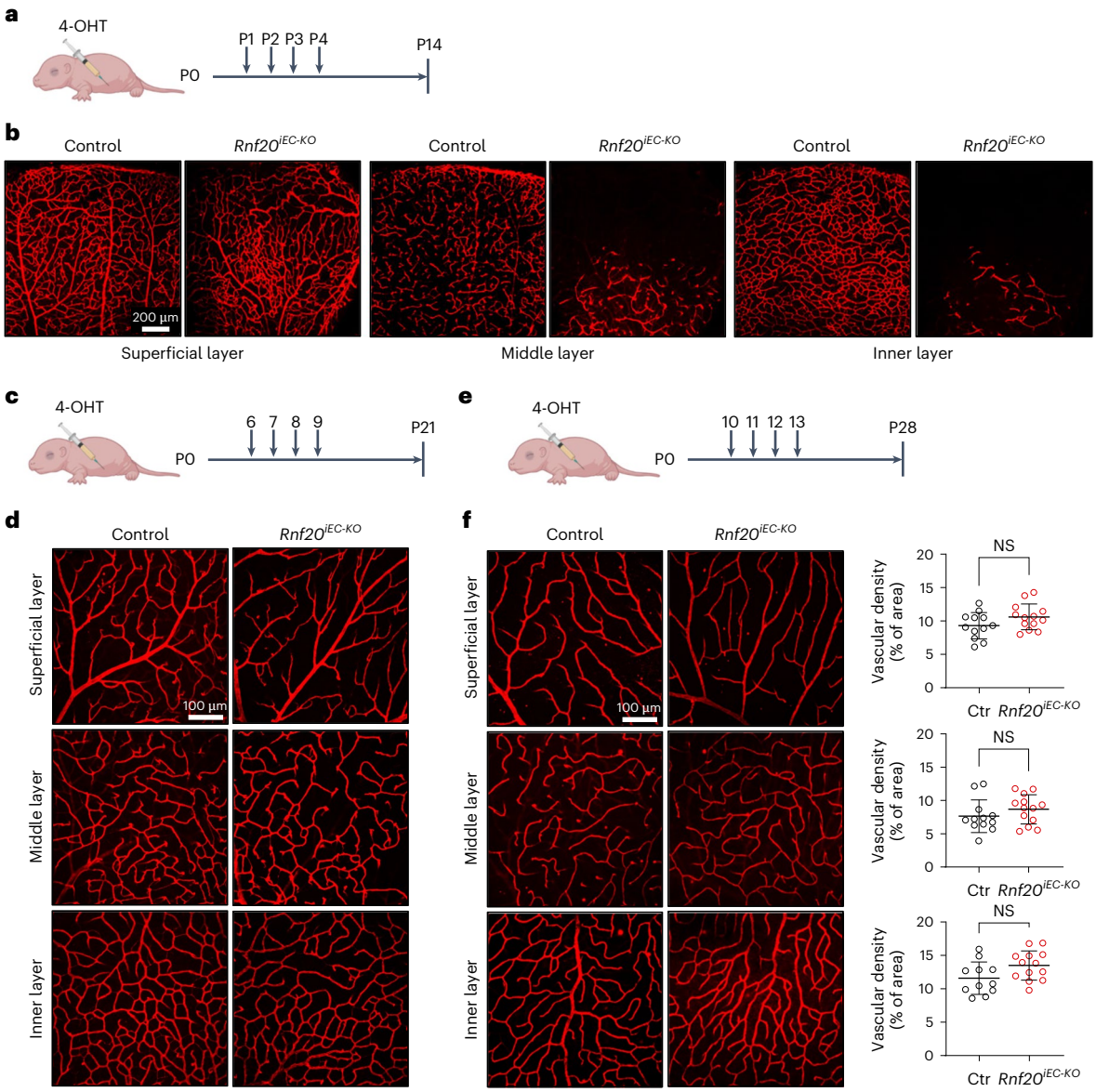

Fig. 2 | Temporal requirement of RNF20 in retinal vessel growth and patterning. a, Schematic representation of the experimental setup in **b**. **b**, Immunostaining for IB4 and confocal images of the superficial (left), middle and deep vascular plexus (right panels) at P14. **c**, Schematic representation of the experimental setup in **d**. **d**, Immunostaining for IB4 and confocal images of the superficial, middle and inner (deep) vascular plexus at P21. **e**, Schematic representation of the experimental setup in **f**. **f**, Immunostaining for IB4 and confocal images of the superficial, middle and inner (deep) vascular plexus at P28 and quantification of the vascular density (right panels); each dot represents quantification from individual leaflets from $n = 6$ retinas for each group. Data in **f** are represented as mean ± s.e.m. Differences between groups were assessed using an unpaired two-tailed Student's *t*-test. NS, not significant.

Notably, the vascular defects of *Rnf20*$^{iEC\text{-}KO}$ mice did not normalize during later phases of retinal development, and, by P14, we observed a substantially altered superficial network and reduced vascular network in the middle and deep vascular plexus (Fig. 2a,b). In contrast, EC-specific *Rnf20* ablation at later timepoints—for example, after the superficial layer has formed—resulted in no major morphogenetic defects (Fig. 2c–f). These results are consistent with the lower expression of *Rnf20* at these stages (Extended Data Fig. 1a). Taken together, our results suggest that RNF20 is an important regulator of vascular morphogenesis in the early postnatal window, acting as a selective suppressor of tip cell state and function.

Rnf20 loss results in Pol II promoter-proximal pause release at highly paused genes

To identify mechanisms underlying RNF20 function in angiogenic growth, we performed RNA-seq of retinal ECs sorted from control and *Rnf20*$^{iEC\text{-}KO}$ mice (Fig. 3a and Extended Data Fig. 2a,b). These analyses identified profound changes in gene expression in RNF20-deficient ECs. Among the upregulated transcripts were genes involved in blood vessel morphogenesis, cell activation and cell motility and MAPK cascade as well as genes involved in negative regulation of cell proliferation, consistent with the observed phenotypic changes (Fig. 3b,c and Source Data Fig. 3). For example, tip cell marker genes such as *Flt4* (*Vegfr3*), *Dll4*, *Esm1* and *Cxcr4*; venous EC marker genes *Nrp2* and *Ephb4*; and the negative regulator of cell proliferation *Cdkn1a* were significantly upregulated in *Rnf20*$^{iEC\text{-}KO}$ ECs (Fig. 3b). In contrast, genes such as *Cc2d2a*, *Ift88*, *Bbs7*, *Arl6* and *Tmem67*, which are involved in the formation and organization of cilia, integral to flow response, were downregulated. Gene set variation analysis (GSVA) revealed that genes upregulated upon *Rnf20* loss are characteristic for tip and venous ECs[25] (Fig. 3d). In contrast, gene signatures of arterial and proliferative ECs were suppressed upon *Rnf20* depletion. Consistent with the RNA-seq

analysis, we observed greatly increased FLT4 and DLL4 protein levels in *Rnf20*$^{iEC\text{-}KO}$ retinas (Fig. 3e).

To understand whether changes in gene expression are simply due to increased tip cell numbers in the developing *Rnf20*$^{iEC\text{-}KO}$ retinas, we performed RNA-seq in human umbilical vein endothelial cells (HUVECs) transfected with control small interferring RNA (siRNA) or siRNA against *RNF20* (Extended Data Fig. 2c–e and Source Data Fig. 3). Similarly to *Rnf20*$^{iEC\text{-}KO}$ ECs, *siRNF20* HUVECs showed overrepresentation of genes involved in cell adhesion and motility and, interestingly, an enrichment of genes involved in the VEGFA–VEGFR2 signaling pathway (Fig. 3f,g). Consistent with the decreased EC proliferation in the developing *Rnf20* LOF retinas, *siRNF20* HUVECs also showed downregulation of cell cycle regulators (Fig. 3f and Extended Data Fig. 2f). RT–PCR analysis further confirmed these transcriptional alterations (Extended Data Fig. 2g). Together, these findings suggest that the morphogenetic defects in the *Rnf20* mutants, particularly the tip cell phenotype, might be linked to aberrant VEGFA signaling.

Because RNF20 has been shown to regulate Pol II activity, we next performed chromatin immunoprecipitation followed by sequencing (ChIP-seq) for total Pol II to calculate the pausing index (PI) in control and *siRNF20* HUVECs (Fig. 3h–j, Extended Data Fig. 2h,i and Source Data Fig. 3). PI, employed as a surrogate for assessing the extent of promoter-proximal Pol II pausing at a gene, was calculated by the ratio of Pol II density at the promoter (−50 bp to +300 bp) over the elongating Pol II at gene bodies (+300 bp to the transcription termination site (TTS) + 3,000 bp) derived from total Pol II ChIP-seq datasets (Fig. 3h). Genes were classified based on their PI in control HUVECs, with highly paused genes categorized in the third quartile (Q3) of the PI distribution. We found a significantly decreased PI at highly paused genes upon RNF20 loss (Fig. 3i), whereas the PI at all genes was slightly but significantly increased, suggesting a role of RNF20 in mediating promoter-proximal pausing at highly paused genes (Fig. 3i). Gene Ontology (GO) analysis of highly paused genes revealed overrepresentation of genes involved in cellular response to stress, including fluid shear stress, VEGFA–VEGFR2 signaling pathway, RNA metabolism and splicing as well as regulation of cell cycle and cell death (Fig. 3j,k and Extended Data Fig. 2i).

Rnf20 loss results in alternative splicing of pro-angiogenic genes, such as VEGFA

Transcriptional elongation by Pol II is coupled to mRNA processing[28], and, therefore, RNF20 LOF might result in alternative splicing. In addition, we also observed genes involved in RNA metabolism and splicing to be paused by RNF20 (Fig. 3k). Thus, we next performed differential splicing analysis using the endothelial in vivo and in vitro RNA-seq datasets. In both, we found a large number of differentially spliced genes (Source Data Fig. 4). Among the differentially spliced and upregulated genes in *Rnf20*$^{iEC\text{-}KO}$ retina ECs were genes involved in extracellular matrix (ECM) organization, VEGFA–VEGFR2 signaling, signaling through tyrosine kinases and genes involved in cell adhesion and cytokine stimulation (Figs. 4a,b and Extended Data Fig. 3a). Among the downregulated and differentially spliced genes were candidates involved in cilium organization. We also found a large number of genes that were differentially spliced but did not show altered expression (Extended Data Fig. 3b). Nevertheless, these alternative splicing events could interfere with protein functions. These genes belonged to the GO terms related to DNA repair, cell cycle, mRNA metabolic process, chromatin organization and mRNA processing (Extended Data Fig. 3b). In this context, RNF20 is required for recruitment of double-strand break (DSB) repair proteins and timely DNA damage repair, and its loss results in accumulation of DNA damage[29,30]. Indeed, RNF20-depleted HUVECs showed increased levels of γH2AX, a marker of DSBs, without any DNA damage-inducing agents (Extended Data Fig. 3c), in concordance with another study showing accumulation of DNA damage in ECs upon *Rnf20* LOF[24].

Notably, *Vegfa* was differentially spliced in control versus *Rnf20*$^{iEC\text{-}KO}$ retina ECs. In control ECs, *Vegfa* coding exons 2–7 were largely excluded, leading to a non-functional transcript, and *Rnf20* deficiency resulted in the inclusion of exons 2–4/5 (Fig. 4c,d). Sanger sequencing of the PCR products resulting from amplification of retinal ECs cDNAs with primers located at the transcription start and end site confirmed the expression of *Vegfa111* and *Vegfa121* isoforms in *Rnf20*$^{iEC\text{-}KO}$ (Fig. 4c,d). Consistent with the increased *Vegfa111* and *Vegfa121* expression, we observed increased total VEGFA protein levels in the retinal vasculature (Fig. 4e). Likewise, silencing of *RNF20* in HUVECs resulted in major changes in VEGFA splicing and other genes involved in the VEGFA–VEGFR2 signaling pathway, tube morphogenesis (including endothelial tube formation), protein catabolic processes and ECM organization (Extended Data Fig. 4f). RT–PCR analysis revealed that *VEGFA111* was highly upregulated, whereas the anti-angiogenic *VEGFA121b* isoform was decreased, upon RNF20 depletion (Fig. 4g). Consistent with the increased expression levels of pro-angiogenic and the decreased expression of anti-angiogenic *VEGFA* isoforms, RNF20-deficient HUVECs were able to sprout even without the addition of VEGFA, and this effect was further enhanced by the presence of exogenous VEGFA (Fig. 4h,i). Taken together, these data emphasize that endothelial RNF20 limits cell-autonomous VEGF signaling. This occurs through transcriptional and post-transcriptional control mechanisms and ensures proper sprouting angiogenesis.

RNF20 modulates the VEGF–Notch signaling circuits during sprouting angiogenesis

Because our results indicated that RNF20 mediates transcriptional pausing at highly paused genes, we next studied whether it integrates signals and TF activities. To this end, we performed assay for transposase-accessible chromatin with sequencing (ATAC-seq) to analyze the accessibility of chromatin within the genome, followed by TOBIAS footprinting analysis[31] (Fig. 5a–c, Extended Data Fig. 4a–c and Source Data Fig. 5). We identified a significant increase in chromatin accessibility at genes involved in cell activation, migration and the VEGFA–VEGFR signaling pathway (Fig. 5a,b), whereas chromatin permissiveness was decreased at genes involved in cytoskeleton-dependent

Fig. 3 | RNF20 induces transcriptional pausing of highly paused genes. **a**, Schematic representation of the experimental setup. FACS, fluorescence-activated cell sorting. **b**, Volcano plot showing the distribution of differentially expressed genes in *Rnf20*$^{iEC\text{-}KO}$ versus control retina ECs. $n = 3$; $\log_2$ fold change ≤ −1, ≥1; $P < 0.05$. Differential expression analysis was performed using DESeq2 (version 1.40.0). Different colored dots represent genes involved in pathways presented in **c**. **c**, Top GO terms of genes upregulated and downregulated upon *Rnf20* loss in retina ECs. **d**, GSVA to calculate gene set scores for EC signature summaries for genes upregulated in *Rnf20*$^{iEC\text{-}KO}$ compared to control retina ECs. **e**, Immunostaining for VEGFR3 (FLT4) (**e**, left) and DLL4 (**e**, right), together with IB4. **f**, Top GO terms of genes upregulated and downregulated upon *RNF20* silencing in HUVECs ($n = 3$; $\log_2$ fold change ≤ −0.58, ≥0.58; $P < 0.05$). **g**, Heatmap representation of overlapping transcriptional changes in mouse retinas and HUVECs upon RNF20 loss. **h**, Schematic representation of Pol II average profiles and the method used for defining the Pol II PI. PI was calculated by the ratio of −50 bp to +300 bp Pol II signal divided by the Pol II signal within +300 bp to the TTS + 3 kb. Highly paused genes were identified as those falling within the third quartile (Q3) of the PI in control HUVECs. **i**, Boxplot showing the minimum, 25th percentile (Q1), median, 75th percentile (Q3) and maximum of Pol II PI after RNF20 depletion in HUVECs for highly paused genes ($n = 3{,}816$) and for all genes ($n = 15{,}455$); $n = 3$ Pol II ChIP-seq for each group. **j**, Genome tracks of merged Pol II ChIP-seq reads in HUVECs transfected with control siRNA or siRNA against *RNF20* ($n = 3$, for each group). **k**, GO analysis of highly paused genes in HUVECs. GO term enrichment analysis in **c**, **f** and **k** was performed using Metascape (version 3.5). The bars represent the $-\log_{10}$(*P* value) for enriched GO terms.

https://doi.org/10.1038/s44161-024-00546-5

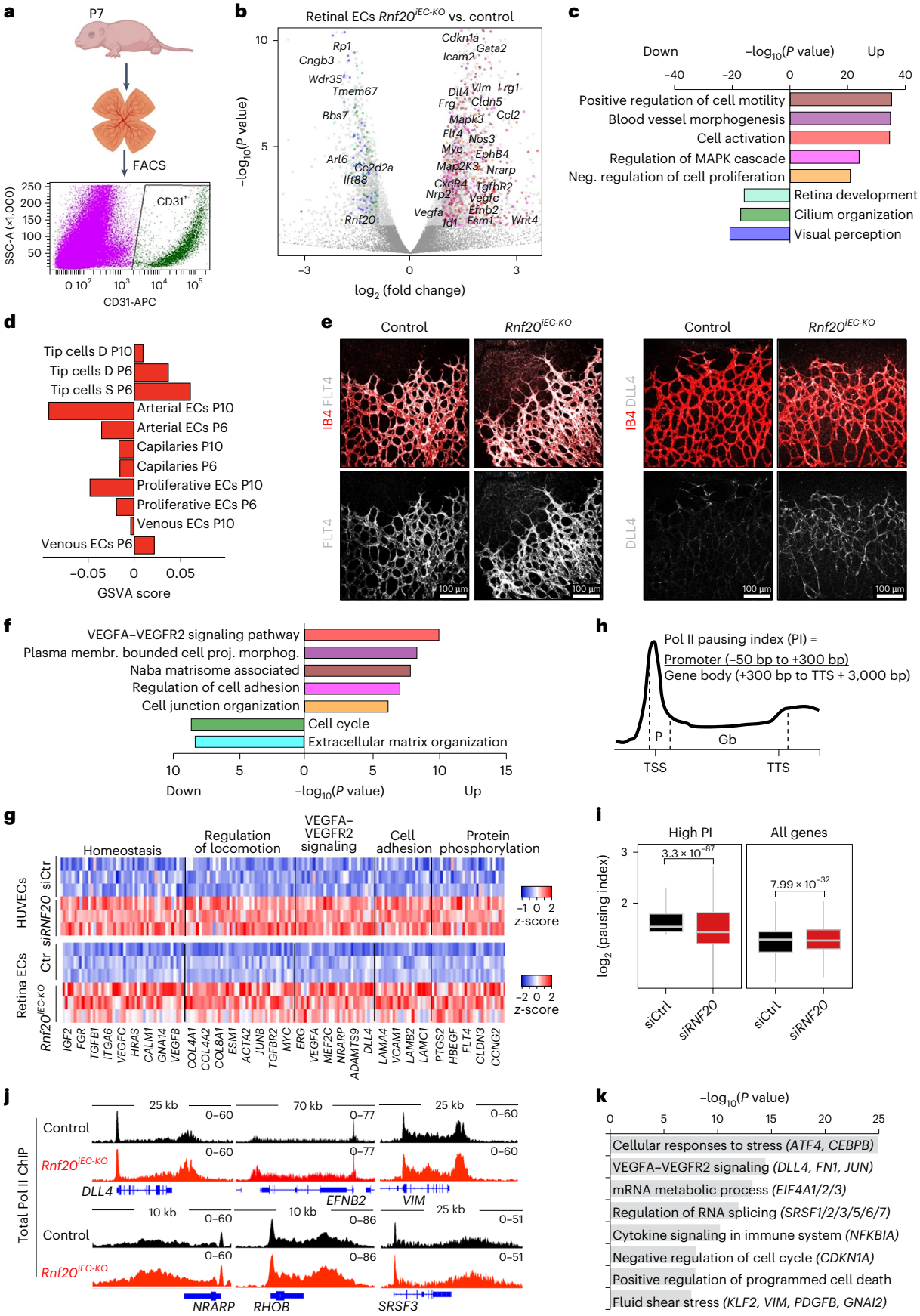

https://doi.org/10.1038/s44161-024-00546-5

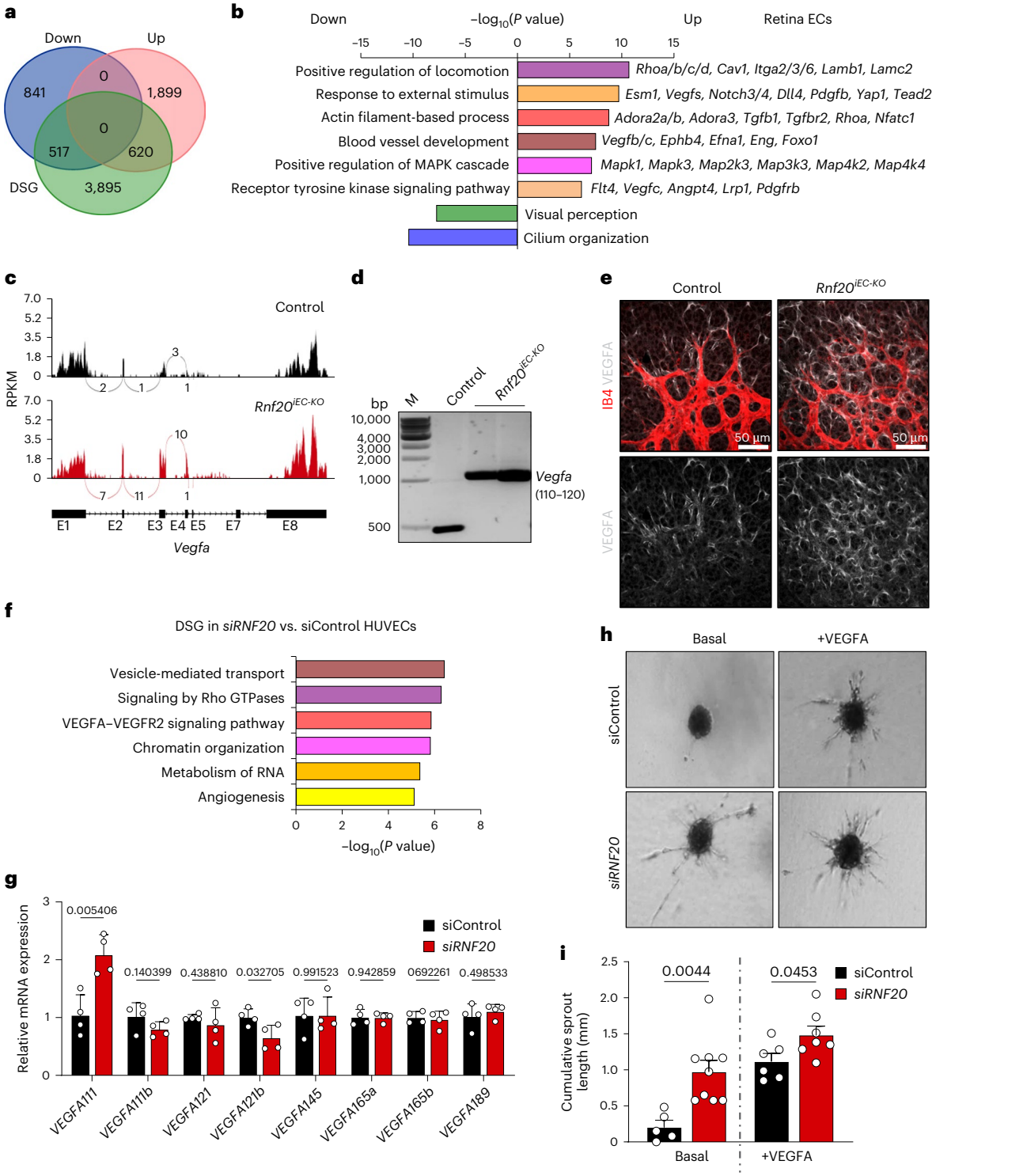

Fig. 4 | RNF20 orchestrates alternative splicing in ECs. a, Venn diagram showing the overlap between differentially expressed genes (upregulated (Up) and downregulated (Down)) and differentially spliced genes (DSGs) ($P < 0.05$, $\log_2$ fold change ≤ −1, ≥1) in *Rnf20*$^{iEC\text{-}KO}$ compared to control retinal ECs. **b**, Top GO terms of DSGs upregulated or downregulated in *Rnf20*-depleted ECs. Representative DSGs in upregulated genes are presented to the right. **c**, Genome tracks of merged RNA-seq reads at the *Vegfa* gene locus in control and *Rnf20*$^{iEC\text{-}KO}$ retinal ECs, showing alternative splicing upon *Rnf20* LOF. **d**, PCR products with primers for amplification of full-length *Vegfa* using cDNA of isolated retinal EC, followed by Sanger sequencing confirming that *Rnf20*$^{iEC\text{-}KO}$ retinal ECs express *Vegfa111* and *Vegfa121*, whereas control ECs express mainly a non-coding transcript. M, marker (DNA). **e**, Immunostaining for VEGFA (white) together with IB4 (red) showing substantially higher VEGFA levels in *Rnf20*$^{iEC\text{-}KO}$ retina. **f**, Top GO terms of DSGs ($P < 0.05$, $\log_2$ fold change ≤ −1, ≥1, $n = 3$) in HUVECs transfected for 60 h with siRNA against *RNF20* versus control siRNA. **g**, qPCR for different *VEGFA* isoforms in HUVECs transfected with control and *RNF20* siRNAs ($n = 4$ biological replicates for each group). **h**,**i**, Sprouting assay with HUVECs transfected with control and *RNF20* siRNA without and with VEGFA supplementation, showing that RNF20-deficient HUVECs sprout without VEGFA addition (**h**) and quantification of the cumulative sprout length (**i**); $n = 5$ siControl basal, $n = 6$ siControl + VEGFA, $n = 9$ *siRNF20* basal and $n = 7$ *siRNF20* + VEGFA (**p**). Data in **g** and **i** are mean ± s.e.m.; differences between groups were assessed using an unpaired two-tailed Student's *t*-test. Numeric *P* values are shown within the figure panels. GO term enrichment analyses in **b** and **f** were performed on DSGs using Metascape (version 3.5). The bars represent the $-\log_{10}$(*P* value) for each enriched GO term.

intracellular transport and cilium organization (Extended Data Fig. 4b,c), in concordance with the observed transcriptomic alterations. Footprinting analysis identified an enrichment of motifs for Ets, Stat and Fos-Jun in *Rnf20*$^{iEC\text{-}KO}$ retinal ECs (Fig. 5c and Extended Data Fig. 4d). In contrast, TF motifs associated with components of the Notch signaling pathway (for example, Hes and Hey) were more frequently identified in open chromatin in control ECs. These data suggest that RNF20 might control the VEGF–Notch signaling circuit during sprouting angiogenesis.

Consistent with the decreased footprints of TFs involved in Notch signaling in the ATAC-seq datasets of *Rnf20*$^{iEC\text{-}KO}$ retinal ECs, we observed a reduced abundance of the Notch1 intracellular domain (N1ICD) on chromatin using cellular fractionation of RNF20-depleted HUVECs (Fig. 5d and Extended Data Fig. 4e). Furthermore, co-immunoprecipitation experiments revealed that RNF20 and N1ICD interact (Fig. 5e), and RNF20 deletion resulted in decreased binding of N1ICD at the promoter of the Notch target gene *HES1* (Fig. 5f) and decreased *HES1* reporter gene activity (Fig. 5g), suggesting that RNF20 might be required for Notch-dependent gene activation. Interestingly, dBre1 (the *Drosophila* homolog of RNF20) was shown to be required for the expression of Notch target genes in *Drosophila* by coupling H2Bub1 to H3K4me3 (ref. 32). Thus, we next performed ChIP-seq for H2Bub1 in control and *siRNF20*-transfected HUVECs (Fig. 5h). We observed significant decrease of H2Bub1 genome wide upon RNF20 depletion, consistent with its function as the main E3 ligase of H2Bub1 (Fig. 5i and Extended Data Fig. 4f). Notably, H2Bub1 levels were more significantly depleted at downregulated genes upon RNF20 LOF, such as *SOX17* and *CCND1*, with particularly significant depletion observed at Notch target genes (Fig. 5h,i and Extended Data Fig. 4f). Consistent with the major decrease in H2Bub1, the expression of these genes was significantly downregulated already 24 h after *RNF20* siRNA transfection (Fig. 5j).

On the other hand, we found enrichment of motifs for ERG, STAT3 and FOSL2, which play important roles in the regulation of VEGFA expression and its downstream effects, at open chromatin regions in *Rnf20*$^{iEC\text{-}KO}$ retinal ECs. TF-gene regulatory network analysis of ERG, STAT3 and FOSL2 footprints suggested that ERG functions upstream of STAT3 and FOSL2 in activating pro-angiogenic genes, such as *Vegfa*, *Vegfc*, *Flt4* and *Nrarp* (Extended Data Fig. 4g). To better discern primary from secondary effects, we conducted ATAC-seq in HUVECs transfected with either control siRNA or siRNA targeting *RNF20*. Comparative analysis of TF motifs enriched in accessible chromatin in both retinal ECs and HUVECs upon RNF20 LOF revealed enrichment of ETS family members in both datasets (Fig. 5k and Extended Data Fig. 4h). In contrast, STAT3 and FOSL2 motifs were exclusively enriched in retinal ECs, indicating an essential role for ETS family members in RNF20 LOF ECs.

Among the ETS family of TFs, ERG was found majorly upregulated in *Rnf20*$^{iEC\text{-}KO}$ retinal ECs (Fig. 3b). ERG is instrumental for EC transcriptional programming[33,34] and regulates Notch signaling and vascular stability[35] but also VEGF-inducible transcription[36]. Analyses of the genome-wide ERG binding profiles[37] revealed significantly higher ERG occupancy at genes upregulated in *RNF20*-deficient HUVECs, including *STAT3*, *FOSL2*, *DLL4*, *VEGFA*, *VEGFC* and *NRARP* (Fig. 5l,m), supporting our footprinting and network analysis. Furthermore, ChIP–qPCR analysis revealed significantly increased binding of ERG at the DLL4, VEGFC and STAT3 regulatory regions upon RNF20 depletion (Fig. 5m,n). ETS1, on the other hand, has been demonstrated to enhance VEGFA-dependent gene expression by promoting the release of paused Pol II (ref. 38).

ERG induces transcriptional pause release at highly paused genes

To further investigate the potential involvement of ETS family members in Pol II pause release after RNF20 LOF, we intersected genes exhibiting ERG (ref. 34) or ETS1 (ref. 38) enrichment at the transcription start site (TSS) (±1 kb) with genes displaying reduced transcriptional pausing in RNF20-depleted HUVECs. Notably, 59% of genes demonstrating decreased Pol II pausing upon RNF20 loss (Fig. 6a) were bound by ERG, ETS1 or both (Fig. 6a,c and Extended Data Fig. 5a). GO analysis of genes bound by both ERG and ETS1, exhibiting decreased pausing in RNF20-depleted HUVECs (825 genes), revealed enrichment in pathways related to VEGFA–VEGFR2 and Rho GTPase signaling, DNA damage response and cell division (Fig. 6b). Genes exclusively bound by ERG (74 genes) were associated with cell cycle checkpoints and division, whereas those bound solely by ETS1 (269 genes) were linked to cell proliferation, tube morphogenesis and VEGFA–VEGFR2 signaling (Extended Data Fig. 5b).

Given that ERG was significantly upregulated in *Rnf20*$^{iEC\text{-}KO}$ retinal ECs (Figs. 3b and 6d) and over 46% of genes exhibiting reduced transcriptional pausing in RNF20-depleted HUVECs were also bound by ERG, we investigated whether elevated levels of ERG might similarly facilitate the release of paused Pol II. To minimize the potential for non-specific effects associated with the shared core DNA binding motif of ETS family TFs, we overexpressed ERG approximately two-fold compared to the control, matching the level of ERG upregulation observed in RNF20 LOF retinal ECs (Fig. 3b). ChIP-seq analysis of total Pol II in both control and ERG-overexpressing HUVECs revealed a significant reduction in Pol II pausing at highly paused genes upon ERG overexpression, with no impact on Pol II distribution across the genome (Fig. 6e). Genes bound by ERG, showing decreased pausing in ERG-overexpressing HUVECs, were associated with chromatin organization, RNA metabolism, DNA damage response, regulation of cellular response to stress as well as nervous system and vasculature development (Extended Data Fig. 5c). Notably, genes bound by ERG exhibiting decreased pausing in both RNF20-depleted and ERG-overexpressing HUVECs were linked

Fig. 5 | RNF20 modulates the VEGF–Notch signaling circuits. a,**b**, Venn diagram showing the overlap between genes characterized by increased chromatin accessibility ($n = 2$, $\log_2$ fold change ≤ −0.58, ≥0.58; $P < 0.05$) and increased expression in *Rnf20*$^{iEC\text{-}KO}$ retina (**a**) and GO analysis of genes within the overlap (**b**). *P* values were calculated using Metascape (version 3.5). **c**, TOBIAS footprinting analysis[31] of control and *Rnf20*$^{iEC\text{-}KO}$ retinal ECs. **d**, Cellular fractioning followed by WB analysis for N1ICD, RBPJ, H2Bub and H2B of control and *RNF20* siRNA-transfected HUVECs. H2B and α-tubulin (TUB) served as loading control. **e**, Co-immunoprecipitation with N1ICD and RNF20. **f**, Relative fold enrichment of N1ICD binding at the *HES1* locus in *siRNF20* versus control HUVECs, determined by N1ICD ChIP–qPCR analysis ($n = 3$). **g**, HES1-luciferase Notch reporter activity in control and *siRNF20* cells transfected with N1ICD ($n = 8$). **h**, Genome tracks of merged H2Bub1 ChIP-seq reads in HUVECs transfected with control and *siRNF20* ($n = 3$ ChIP-seq per group). **i**, Bar plot showing the statistical significance ($-\log_{10}$(*P* value)) of H2Bub1 decrease in *siRNF20* versus control HUVECs on the gene body of hg38 genome-wide transcriptome, at downregulated upon RNF20 LOF genes and at Notch target genes (GO:0007219). **j**, qPCR for Notch target genes (*HES1*, *HES2*, *HEY1* and *NOTCH3*) as well as other downregulated upon RNF20 LOF genes, such as *CCND1* and *SOX17*, in HUVECs transfected with control and *siRNF20* for 24 h ($n = 3$). **k**, Statistical significance ($-\log_{10}$(*P* value) > 50) of differential TF motifs at ATAC-seq peaks in *Rnf20*$^{iEC\text{-}KO}$ versus control retinal ECs ($n = 2$) and in si*RNF20* versus control HUVECs ($n = 4$). Statistical significance was assessed using TOBIAS (version 0.14.0). **l**, Line plots representing the average ERG ChIP-seq read density (RPM) at TSS ± 2 kb of genes upregulated, downregulated or non-changed (NC) in *siRNF20* HUVECs ($n = 4$). Shaded areas represent the ±s.e.m. **m**, Genome tracks of ERG ChIP-seq reads at RNF20-dependent genes. Primers used for the ChIP–qPCR analysis in **n** are indicated with a black bar. **n**, Relative fold enrichment of ERG binding in *siRNF20* versus control HUVECs, determined by ChIP–qPCR analysis ($n = 4$). Data in **f**, **g**, **j** and **n** represent mean ± s.e.m.; differences between groups were assessed using an unpaired two-tailed Student's *t*-test. Differences in **i** and **l** were calculated using a two-sided Wilcoxon test. Numeric *P* values are shown within the figure panels. CTRL, control; KO, knockout; RPM, reads per million.

https://doi.org/10.1038/s44161-024-00546-5

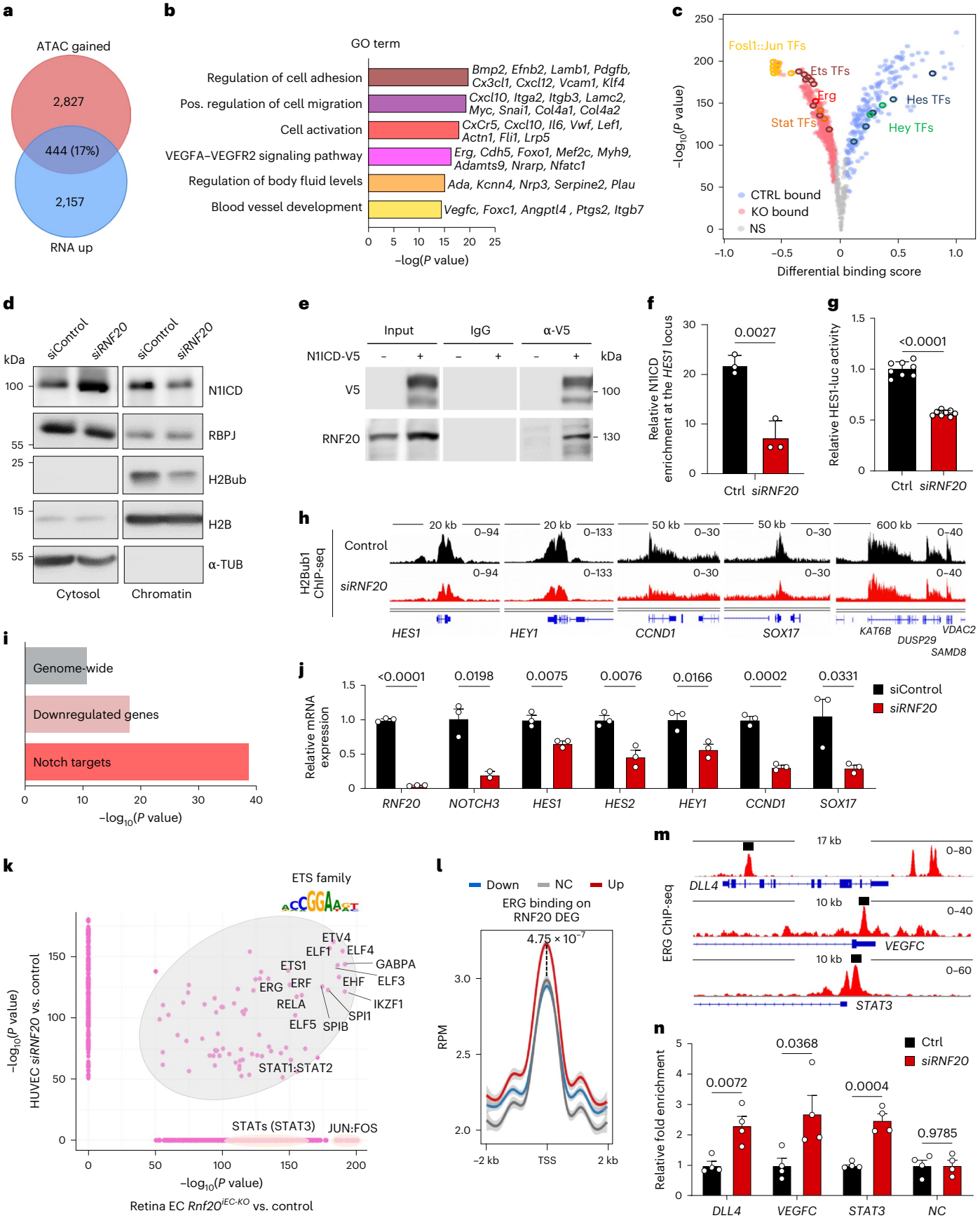

https://doi.org/10.1038/s44161-024-00546-5

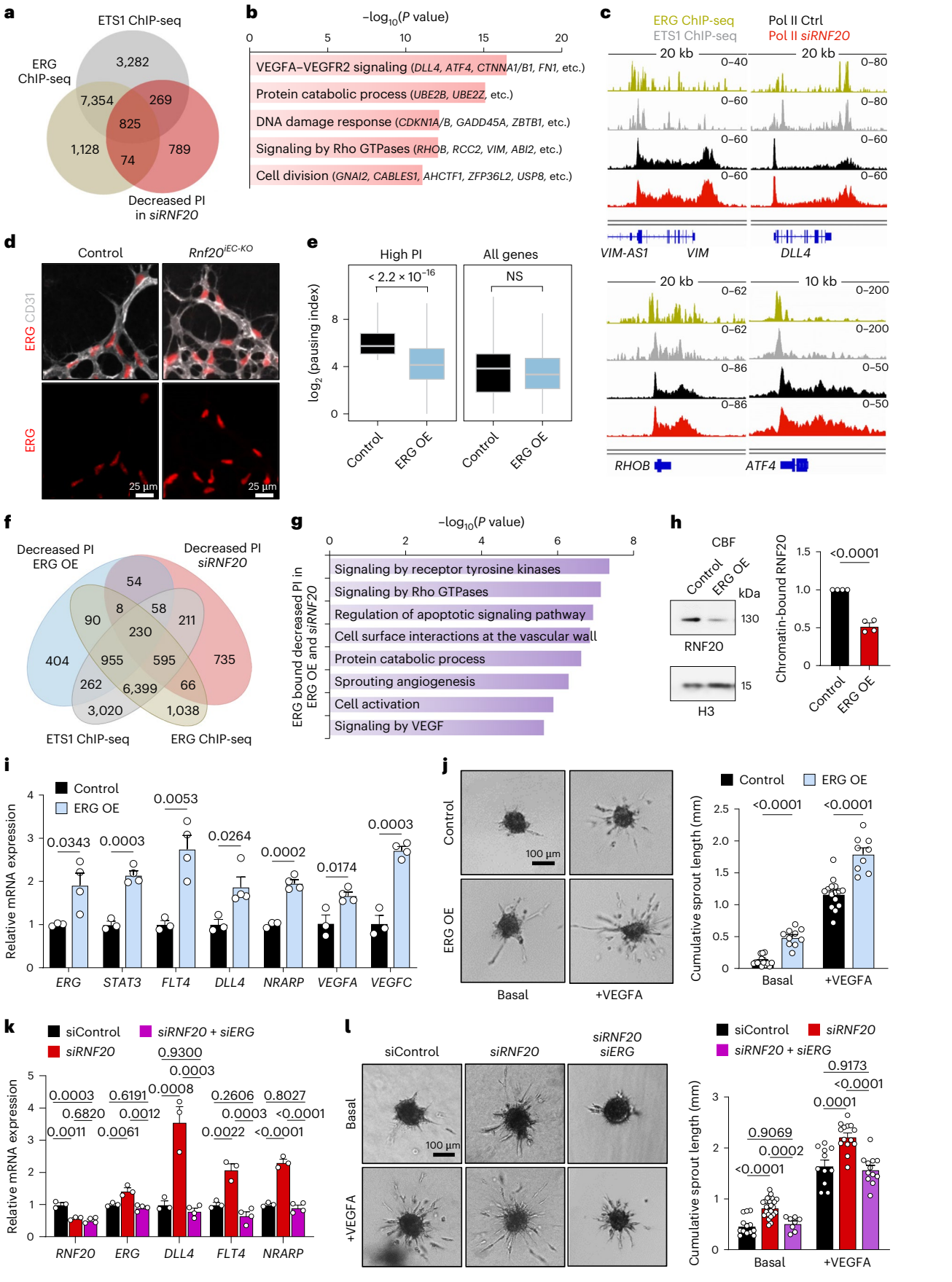

Fig. 6 | ERG induces transcriptional pause release at highly paused genes. **a**, Overlap of genes bound by ETS1 (ref. 38) or ERG (ref. 34) at the TSS (±1 kb) with genes showing decreased PI in HUVECs transfected with *siRNF20* versus control siRNA. **b**, GO analysis of genes bound by both ERG and ETS1 and showing decreased PI upon RNF20 loss. **c**, Genome tracks of ERG and ETS1 ChIP-seq reads and merged total Pol II ChIP-seq reads in control ($n = 3$) and *siRNF20* ($n = 3$) HUVECs. **d**, Images of ERG and CD31 immunostaining of control and *Rnf20*$^{iEC\text{-}KO}$ retinas. **e**, Box plot showing the minimum, 25th percentile (Q1), median, 75th percentile (Q3) and maximum of Pol II PI after ERG overexpression in HUVECs for highly paused genes ($n = 3{,}554$) and for all hg38 genes. **f**, Overlap of genes bound by ETS1 or ERG at the TSS (±1 kb) with genes showing decreased PI in *siRNF20* versus control HUVECs ($n = 3$) or ERG-overexpressing (OE) versus control HUVECs ($n = 2$ ChIP-seq per group). **g**, GO analysis of genes bound by ERG and showing decreased PI upon both ERG overexpression and RNF20 depletion. **h**, Cellular fractioning of control and ERG-OE HUVECs, followed by WB analysis for RNF20 and H3 (loading control) in the chromatin-bound fraction (CBF) and quantification ($n = 4$) to the right. **i**, qPCR analysis of RNF20-dependent genes in control ($n = 3$) and ERG-OE ($n = 4$) HUVECs. **j**, Sprouting assay with HUVECs (left) and quantification of the cumulative sprout length (right). Basal: siControl ($n = 15$) and ERG OE ($n = 10$); +VEGFA: siControl ($n = 15$) and ERG OE ($n = 9$). **k**, qPCR analysis of HUVECs transfected with control ($n = 3$), with *RNF20* siRNAs alone ($n = 3$) or with 1-nm *ERG* siRNA to reduce ERG levels in RNF20-depleted HUVECs to control levels ($n = 4$ *siRNF20* + *siERG*). **l**, Sprouting assay (left) and quantification of the cumulative sprout length (right). Basal: siControl ($n = 13$), *siRNF20* ($n = 26$), *siERG* ($n = 9$) and *siRNF20* + *siERG* ($n = 8$); +VEGFA: siControl ($n = 11$), *siRNF20* ($n = 14$), *siERG* ($n = 13$) and *siRNF20* + *siERG* ($n = 12$). Data in **h**, **i** and **j** represent mean ± s.e.m.; differences between groups were assessed using an unpaired two-tailed Student's *t*-test. Data in **k** and **l** represent mean ± s.e.m.; differences between groups were assessed using one-way ANOVA multiple comparisons test. *P* values in **b** and **g** were calculated using Metascape (version 3.5).

to receptor tyrosine kinase signaling, signaling by Rho GTPases and VEGFA, cell activation and sprouting angiogenesis (Fig. 6f,g). Consequently, we further investigated whether and how the increased levels of ERG contribute to the transcriptional alterations and enhanced sprouting observed in RNF20-depleted HUVECs. Interestingly, overexpression of ERG in HUVECs, at levels similar to Rnf20-deficient ECs, led to significantly decreased binding of RNF20 to chromatin, despite the increased *RNF20* mRNA expression (Fig. 6h and Extended Data Fig. 5d). This suggests that increased ERG levels restrict RNF20 binding to chromatin. Notably, ERG overexpression increased expression of RNF20-repressed genes (Fig. 6i) and increased sprouting in basal medium, similarly to RNF20-deficient HUVECs (Fig. 6j). Furthermore, reducing ERG levels in RNF20-depleted HUVECs to those seen in controls normalized the transcriptional changes dependent on ERG and reduced the excessive sprouting in response to RNF20 LOF (Fig. 6k,l). Further reduction of ERG levels resulted in significantly lower expression of *DLL4* and *NRARP*, whereas ETS1 silencing had a less pronounced effect (Extended Data Fig. 5e).

Taken together, these results suggest that ERG plays a major role in mediating the transcriptional and functional alterations of RNF20-deficient ECs.

Blocking the VEGF–ERK1/2 axis inhibits tip cell acquisition after RNF20 LOF

Because the VEGFA–VEGFR signaling pathway was highly enriched in all datasets, we next assessed the downstream signaling events. Interestingly, *siRNF20* HUVECs grown in basal medium showed significantly higher levels of VEGFR2 and p^{Tyr1175}-VEGFRTyr1175 as well as increased levels of activated Thr202/Tyr2 phosphorylated (p-) ERK1/2 and higher expression of the RNF20-dependent gene DLL4 (Fig. 7a,b), whereas activated p-p38 levels were not significantly affected. Either silencing of VEGFR2 or pharmacological inhibition of p-ERK1/2 with the MEK inhibitor (MEKi) PD0325901 resulted in decreased protein levels of the RNF20-dependent genes, DLL4 and VEGFR3 (Fig. 7c,d and Extended Data Fig. 6a,b). Furthermore, treatment of control and *siRNF20* HUVECs with the VEGFR2 signalling inhibitor vandetanib or the MEKi PD0325901 decreased sprouting of *RNF20*-depleted HUVECs (Fig. 7e and Extended Data Fig. 6c,d). Because ERG activity was shown to be regulated by VEGF/MAPK/ERK signaling[36], activation of the VEGFA–ERK1/2–ERG axis might be responsible for the pro-angiogenic activity of RNF20-depleted ECs. Next, we sought to corroborate our findings in vivo either by blocking VEGFR2 signaling using the anti-VEGFR2 antibody DC101 or by pharmacological inhibition of ERK phosphorylation using the MEKi SL327. Both treatments normalized the number of tip cells and number of filopodia in *Rnf20*$^{iEC\text{-}KO}$ similar to control retinas (Fig. 7f–i and Extended Data Fig. 6e–h), emphasizing that increased VEGFA signaling through ERK1/2 activation plays an instrumental role in the cellular phenotypes caused by endothelial *Rnf20* loss.

Discussion

Our work uncovered a crucial role of RNF20 in the regulation of the VEGF–Notch signaling circuits orchestrating EC state transitions, which are the driving force for angiogenic growth and physiological tissue repair but also for pathological angiogenesis (Fig. 7j and Extended Data Fig. 7).

Our data show that RNF20 mediates Pol II promoter-proximal pausing specifically at genes that are highly paused in ECs. These genes play crucial roles in various cellular processes, including the cellular response to fluid shear stress, the VEGFA–VEGFR2 signaling pathway, cell cycle regulation, cell death and RNA metabolism/splicing. Notably, consistent with the rapid transcriptional changes observed in genes encoding splicing factors, we observed substantial alterations in RNA splicing. Additionally, Pol II elongation rate, also termed transcription speed or velocity, influences splicing-related processes, such as constitutive splicing, alternative splicing and back-splicing[39]. H2Bub1 is closely linked to Pol II elongation rate[40]; therefore, it is plausible that

Fig. 7 | Activation of the VEGF–ERK1/2 signaling axis upon RNF20 loss results in increased tip cell numbers. **a**,**b**, WB analysis for RNF20, DLL4, activated Thr1175 phosphorylated VEGFR2, total VEGFR2, activated Thr202/Tyr2 phosphorylated ERK1/2, total ERK1/2, activated Thr180/Tyr182 phosphorylated p38, total p38 as well as the loading control α-tubulin of HUVECs transfected with control and *RNF20* siRNA (**a**) and quantification of protein levels (**b**); $n = 7$ siControl, $n = 7$ *siRnf20* for VEGFR2; $n = 7$ siControl, $n = 7$ *siRnf20* for pVEGFR2; $n = 8$ siControl, $n = 8$ *siRnf20* for pERK1/2. **c**, WB analysis for RNF20, VEGFR2, VEGFR3, pERK$^{Thr202/Tyr204}$, DLL4 and α-tubulin (TUB) of total protein extracts of HUVECs transfected with control, *VEGFR2* and *RNF20* siRNA. **d**, WB analysis for RNF20, VEGFR2, VEGFR3, pERK$^{Thr202/Tyr204}$, DLL4 and α-tubulin of total protein extracts of HUVECs transfected with control or *RNF20* siRNA and treated with either DMSO or the MEKi PD0325901 for 24 h. **e**, Sprouting assay with HUVECs transfected with control or *RNF20* siRNA and treated with DMSO, the VEGFR inhibitor vandetanib (ZD6474) or the MEKi PD0325901 cultured in basal medium without VEGFA supplementation (left) and quantification of the cumulative sprout length (right) ($n = 10$ for siControl, siControl + vandetanib, siControl + MEKi, $n = 18$ for *siRNF20*, $n = 10$ for *siRNF20* + vandetanib, *siRNF20* + MEKi). **f**,**g**, Immunostaining for CD31 and ESM1 in control and *Rnf20*$^{iEC\text{-}KO}$ retinas treated with either PBS or DC101 (**f**) or with oil and the MEKi SL327 (**g**). **h**,**i**, Quantification of tip cells per area of vascular coverage in control and *Rnf20*$^{iEC\text{-}KO}$ retinas treated with either PBS or DC101; each data point represents different leaflets from $n = 4$ Control + PBS, $n = 6$ *Rnf20*$^{iEC\text{-}KO}$ + PBS, $n = 6$ Control + DC101, $n = 6$ *Rnf20*$^{iEC\text{-}KO}$ + DC101 retinas (**h**) or with oil and the MEKi SL327; $n = 4$ Control + oil, $n = 4$ *Rnf20*$^{iEC\text{-}KO}$ + oil, $n = 2$ Control + SL327, $n = 4$ Rnf20$^{iEC\text{-}KO}$ + SL327 retinas (**i**). **j**, Schematic representation of the molecular and cellular changes resulting from RNF20 loss. Data in **b** and **e** represent mean ± s.e.m.; differences between groups were assessed using an unpaired two-tailed Student's *t*-test. Data in **h** and **i** represent mean ± s.e.m.; differences between groups were assessed using two-way ANOVA with Tukey's correction. Numeric *P* values are shown within the figure panels.

https://doi.org/10.1038/s44161-024-00546-5

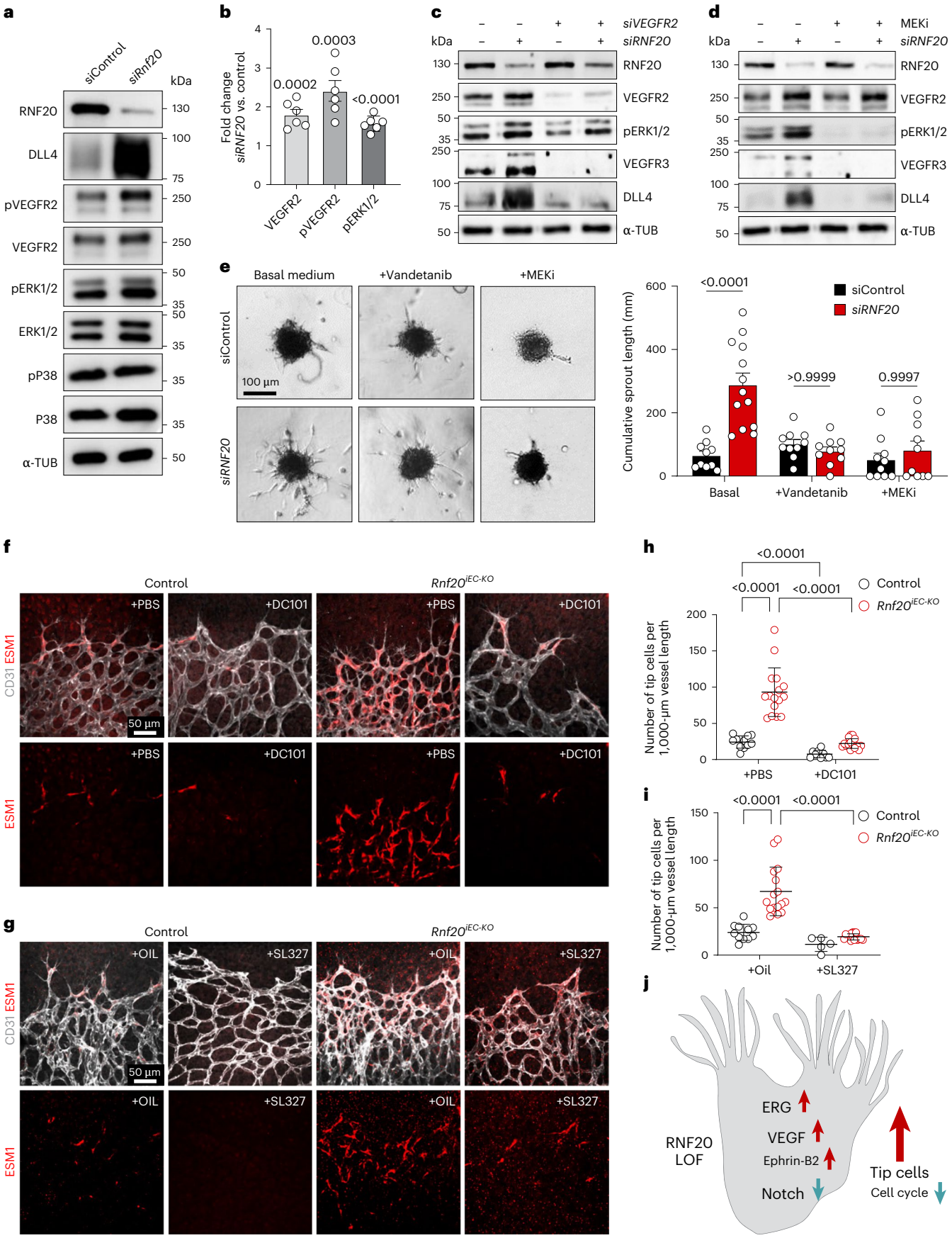

RNF20 regulates RNA diversity by tightly controlling Pol II pause release at genes involved in the regulation of splicing and/or by the regulation of H2Bub1 levels. Specifically, RNF20 LOF resulted in significant changes in the splicing of the critical regulator of angiogenesis and EC behavior, VEGFA. Alternative mRNA splicing of VEGFA gives rise to many isoforms that show different affinities to their receptors, diffusion properties, stabilities and cellular functions[41–43]. Notably, we found increased levels of *VEGFA111* in RNF20-depleted HUVECs and in *Rnf20*$^{iEC\text{-}KO}$ retinal ECs, accompanied by elevated VEGFA protein levels. *VEGFA111* encodes a freely diffusible and stable VEGF isoform lacking the heparin-binding ability encoded by exons 6 and 7 as well as the major proteolytic cleavage sites encoded by exon 5, thereby displaying resistance to proteolysis[41]. *VEGFA111* is highly increased in ECs from *Dll4* LOF retinas, which exhibit increased tip cell formation and enhanced sprouting angiogenesis[7]. This isoform is also specifically induced by genotoxic stress[41], which significantly alters alternative splicing[44]. Notably, RNF20 is required for recruitment of DSB repair proteins and timely DSB repair[29,30], and RNF20 depletion in ECs results in DNA damage[24]; thus, it would be interesting to explore to what extent DNA damage induced by RNF20 loss, or by other stressors such as hypoxia, contributes to VEGFA splicing specifically as well as to RNA diversity in general. Recombinant VEGFA111 binding to VEGFR2 was shown to signal specifically through ERK1/2 activation to regulate EC proliferation, migration, sprouting and EC fate choices[41,45]. Our data indicate that elevated VEGFA signaling, followed by activation of the ERK1/2 signaling cascade and ETS family members, plays a central role in activating pro-angiogenic genes and promoting sprouting upon RNF20 loss.

ETS1 has been demonstrated to boost VEGFA-dependent gene expression by facilitating the release of paused Pol II through the recruitment of the positive elongation factor P-TEFb[38]. Our study uncovered that increasing ERG levels can also effectively trigger the release of paused Pol II by displacing RNF20 from highly paused genes. Although our analysis focused on TSSs, it is important to note that ERG also regulates endothelial gene expression by binding to enhancers[34]. Enhancer-bound TFs can also stimulate Pol II pause release through enhancer–promoter loops[46]. Thus, ERG might promote Pol II pause release by engaging with enhancers and facilitating enhancer–promoter interactions through homodimerization or heterodimerization with other proteins, including other members of the ETS family. In our study, we limited ERG overexpression to approximately two-fold to minimize potential non-specific effects due to the shared core DNA binding motif of ETS family TFs; however, this limitation should be considered when interpreting the results. Notably, ERG appears to play a dominant role in mediating the phenotype in the context of RNF20 LOF. Genes showing increased Pol II release upon ERG overexpression and after RNF20 depletion were associated with receptor tyrosine kinase signaling, signaling by Rho GTPases and VEGFA, cell activation and sprouting angiogenesis. This finding aligns with the role of ERG in dynamically regulating VEGF-inducible genes[36]. Given the substantial transcriptional changes observed with RNF20 loss, the combination of RNF20 depletion and increased ERG activity may synergistically enhance VEGFA-dependent gene expression.

Together with elevated VEGF signaling, we observed decreased Notch signaling. The *Drosophila* homolog of RNF20, dBre1, has been shown to be required for the expression of Notch target genes by coupling H2Bub1 to H3K4me3 (ref. 32). Similarly, we observed that the mammalian RNF20 plays a crucial role in regulating Notch target gene expression. We found that N1ICD interacts with RNF20, and depletion of RNF20 led to a global reduction in N1ICD association to chromatin and major decrease of H2Bub1 levels at Notch target genes in ECs, suggesting an evolutionary conserved role of RNF20 in the regulation of Notch-dependent transcriptional program through modulating the histone code. On the other hand, Dll4 and Nrarp, targets of both ERG and Notch[34,47], were among the most upregulated genes upon *Rnf20* loss. ERG interacts with N1ICD[35], suggesting that elevated ERG levels may be responsible for the increased expression of a subset of Notch target genes upon RNF20 LOF. Nrarp is known to inhibit the transcription of Notch target genes[48,49], either by forming an inhibitory complex with CSL–NICD or by destabilizing NICD. Thus, its increased expression may also contribute to the attenuated Notch signaling observed in *Rnf20*$^{iEC\text{-}KO}$ ECs.

Finally, we found consistently higher total levels of VEGFR2, which were not affected by ERK1/2 inhibition. The *Vegfr2* promoter is repressed by Hes and NICD[50]. Thus, the inability of these factors to bind to chromatin might be responsible for the high level of VEGFR2 expression and the further potentiation of VEGF signaling. Additionally, ephrin-B2, which enables VEGF receptor endocytosis and downstream signal transduction[51], is a highly paused gene significantly upregulated in RNF20-depleted HUVECs and in *Rnf20*$^{iEC\text{-}KO}$ retinal ECs. Thus, because VEGFA and VEGFC levels, as well as their receptors and their signal transduction ability, are increased in RNF20 LOF ECs, our model suggests that exacerbation of VEGF–VEGFR levels results in uncontrolled tip cell specification. Notably, our data emphasize that the increased number of tip cell-like ECs upon *Rnf20* loss occurs independently of EC proliferation. Indeed, *Rnf20*-defcient ECs showed significantly decreased proliferation, which is likely a consequence of excessive VEGFA/C levels above the threshold levels. High mitogenic VEGF stimulation has been proposed to induce cell cycle arrest in angiogenic vessels through p-ERK-dependent upregulation of p21 (ref. 8). *CDKN1A*, encoding p21, belongs to the highly paused genes in ECs, which are released for active elongation upon RNF20 loss, providing a possible explanation for the decreased proliferation but increased tip cell specification in *Rnf20*$^{iEC\text{-}KO}$ mutants. Additionally, we observed defective reverse migration and compromised artery formation upon *Rnf20* LOF. High ephrin-B2 expression in tip cells promotes arterial specification, which involves Notch activation and Sox transcription factor activity[10]. Exploring to what extent decreased Sox17 levels, Notch signaling activity, altered shear stress response or cilia dysfunction upon RNF20 LOF compromises artery formation would be interesting for future studies.

Interestingly, mutations in the *RNF20* gene have been associated with cardiovascular malformations in human patients[23], and *RNF20* levels are altered in many cancers[52]. Beyond ECs, RNF20 may, therefore, play a broader role in controlling the VEGF–NOTCH signaling circuit, leading to cardiovascular and cancerous diseases when the function of this E3 ubiquitin ligase is corrupted. Delineating the mechanisms that control RNF20 expression and activity might, thus, provide insights into diseases caused by vascular dysfunction.

Methods

Mouse lines

The *Rnf20tm1a(EUCOMM)Wtsi* line was generated by microinjection of *Rnf20 tm1a(EUCOMM)Wtsi* embryonic stem cells, obtained from the European Conditional Mouse Mutagenesis Program (EUCOMM), into blastocysts (Extended Data Fig. 1a). For the generation of a conditional (floxed) allele *Rnf20tm1c(EUCOMM)Wtsi* line, the *Rnf20tm1a(EUCOMM)Wtsi* mouse line was crossed with germline FLP deleter mouse line. To induce endothelial-restricted deletion, the resulting *Rnf20tm1c(EUCOMM)Wtsi* mice carrying a conditional floxed allele were bred to a line carrying the tamoxifen-inducible recombinase CreERT2 driven by the platelet-derived growth factor subunit B (Pdgfb) promoter—that is, *Pdgfb-iCreERT2* (ref. 53). To activate CreERT2, pups were administered 25 µl of 3 mg ml^{-1} 4OHT (Sigma-Aldrich, H7904) intraperitoneally from P1 to P4. Retinas were harvested between P7 and P28. Mice analyzed in this study were on a C57BL/6J background.

Animal experiments

All animal experiments were performed according to the regulations issued by the Committee for Animal Rights Protection of the State of

Baden-Württemberg (Regierungspraesidium Karlsruhe; experimental protocol Az.: 35-9185.81/G-181/17).

Whole-mount immunofluorescence staining

Whole-mount immunofluorescence stainings were performed according to ref. 54. In brief, enucleated eyes were fixed in 4% paraformaldehyde (PFA) either for 2.5 h on ice (for stainings: PECAM1, ESM1, FLT4, ICAM2) or for 30 min at room temperature, followed by retina dissection. After dissection, retinas were incubated in blocking buffer (3% FBS, 1% BSA, 0.25% Tween 20, 0.25% Triton X-100, 0.01% sodium deoxycholate in PBS) for 1 h at room temperature. Primary antibodies were incubated in blocking buffer or in blocking buffer diluted 1:1 in PBS (for stainings: PECAM1, ESM1, FLT4, ICAM2) overnight at 4 °C. After three washes with PBST (0.1% Tween 20 in PBS), retinas were then incubated with Alexa Fluor–conjugated secondary antibodies either in modified PBLEC buffer (1 mM $CaCl_2$, 1 mM $MgCl_2$, 0.1 mM $MnCl_2$, 0.5% Triton X-100) or in blocking buffer diluted 1:1 in PBS (for stainings: Pecam1, Esm1, Flt4, Icam2) for 2 h at room temperature. Next, retinas were washed and flat mounted with ProLong Gold antifade mountant (Life Technologies, P36930). For staining with IB4 alone, dissected retinas were blocked and stained in PBLEC buffer (1 mM $CaCl_2$, 1 mM $MgCl_2$, 0.1 mM $MnCl_2$, 1% Triton X-100) for 2 h at room temperature or overnight at 4 °C. EdU incorporation was detected, after injecting pups with 225 µg of EdU in 50 µl of PBS 4 h before harvest, using a Click-iT EdU kit (Thermo Fisher Scientific, C10337) according to the manufaturer's instruction. For details on antibody dilutions, see Extended Data Table 1.

Images were acquired with a Zeiss LSM 700 confocal microscope or Axio Scan.Z1. To compare signal intensities between different groups, settings (laser excitation and detection) were kept constant. FIJI/ImageJ (version 1.53) and Zeiss ZEN software (version 2.3) were used for image acquisition and processing.

Quantitative analysis of the retinal vasculature

Endothelial density analysis was performed with the FIJI/ImageJ plugin Vessel analysis. The number of tip cells was quantified by ESM1/ERG double-positive cells, normalized to the length of the angiogenic front and defined by a line at the base of the tip cells. Filopodia per vessel length were analyzed by the number of filopodia normalized to the length of the angiogenic front, defined by a line at the base of the tip cells per field. Vessel (artery and vein) length was normalized to radial length. EC proliferation was measured by the number of EdU/ERG double-positive cells to the total number of ERG-positive cells per field.

The '*n*' number stands for the number of retinas characterized, which were derived from at least two litters. Individual dots represent measurement data from images taken from different leaflets of each retina.

Cell lines, cell culture and treatments

HUVECs from pooled donors were purchased from Lonza (CC-2519) or PromoCell (C-12208) and cultured in complete EGM-MV2 medium (PromoCell, C-22022) supplemented with 1× penicillin–streptomycin. Human embryonic kidney (HEK293T) cells were purchased from Life Technologies (Thermo Fisher Scientific, R70007) and cultured in DMEM high-glucose GlutaMAX (Gibco, 61965059) supplemented with 10% FBS, 1× penicillin–streptomycin and 1× sodium pyruvate.

Silencing using RNA interference

siRNA-mediated knockdown of *RNF20* was performed by transfection of ON-TARGETplus Human RNF20 siRNA (Dharmacon/Horizon, L-007027-00-0005) or ON-TARGETplus Non-targeting Control siRNA as a control, using Lipofectamin RNAiMAX (Thermo Fisher Scientific, 13778075) according to the manufacturer's instructions with the following modifications: 30 nM siRNA (final concentration) was transfected with 2 µl of Lipofectamine RNAiMAX reagent in 1 ml of complete EGM-MV2 medium (final volume 1.4 ml) per well of a six-well plate overnight. The next day, cells were supplemented with fresh medium, followed by starvation in EGM-MV2 basal medium supplemented with 2% heat-inactivated FBS for 6–8 h before harvesting them at 60–72 h after transfection, for either RNA or protein analysis. For knockdown of ERG, STAT3 or VEGFR2, 1 nM or 15 nM siERG as indicated in the figure legends (siRNA1:CAGAUCCUACGCUAUGGAGUA, siRNA2:ACUCUCCACGGUUAAUGCAUGGUAG mixed 1:1, Sigma-Aldrich) siRNA, 7.5 nM STAT3 (CACAUGCCACUUUGGUGUUUCAUAA) siRNA or 30 nM VEGFR2 siRNA (Dharmacon/Horizon, L-003148-00-005) was used, respectively.

Lentivirus generation and HUVEC transduction

For ERG overexpression in HUVECs, HEK293T cells were transfected with 70% confluency in six-well plates with control plasmid or ERG overexpression plasmid (TRCN0000465638), obtained from the TRC3puro overexpressing library, along with 1 µg of CMVΔR8.74 packaging plasmid and 0.5 µg of VGV.G envelope plasmids using X-tremeGENE DNA transfection reagent (Roche, 6366236001) in 1 ml of complete EGM-MV2 medium (final volume 1.2 ml). The next day, an additional 1 ml of medium was added to the cells. Forty-eight hours after transfection, the viral supernatant was collected, and 100–250 µl of virus was used to transduce HUVECs at 70% confluency in six-well plates overnight in the presence of 8 µg ml^{-1} polybrene (Sigma-Aldrich, TR-1003-G). Seventy-two hours after transduction, HUVECs were harvested for RNA and protein analysis or used for the spheroid sprouting assay.

Spheroid sprouting assay

The spheroid sprouting assay was performed according to ref. 55 with the following modifications. Twenty-four hours after transfection of HUVECs, spheroids were formed in growth medium containing 20% methylcellulose solution (1.2% (w/v) methylcellulose in EGM basal medium) with the hanging drop method for the next 24 h. For embedding the spheroids in collagen gels, a 2.8 mg ml^{-1} collagen solution containing Rat Tail Collagen Type I (Corning, 354249), 10× M199 medium (Gibco, 11825015) and NaOH in a ratio 8:1:1 was mixed 1:1 with the methylcellulose solution containing 20% heat-inactivated FBS to obtain a final collagen concentration of 1.4 mg ml^{-1}. Then, 1 ml of the prepared collagen/methylcellulose solution was mixed with approximately 60 spheroids containing the test substances and immediately transferred to a well in a pre-heated 24-well plate to polymerize for 30 min at 37 °C. After polymerization, 100 µl of basal medium was added on top of the collagen gels, and the spheroids were incubated for 24 h at 37 °C (5% CO_2, 100% humidity). After fixation with 4% PFA, images were acquired with a Leica DMI8 microscope (×10 objective magnification), and the length of the sprouts was measured with FIJI/ImageJ software (calculated as cumulative sprout length). At least 10 spheroids were analyzed for each group.

WB

For whole-cell protein isolation, cells were collected and lysed in RIPA buffer supplemented with protease and phosphatase inhibitor cocktail (Millipore, 535142 and 524632). Protein concentration was quantified using a Pierce BCA protein assay kit (Pierce Biotechnology, 23225).

For protein fractionation, cells were lysed on the plate in lysis buffer (10 mM Tris-HCl (pH 8.0), 10 mM NaCl, 0.2% NP-40, 1× protease inhibitor; approximately 50 µl per 1×10^6 cells) by incubation for 15 min on ice. After centrifugation at 2,500*g* for 5 min at 4 °C, the supernatant containing the cytoplasmic fraction was collected. The cell pellet was washed another three times with lysis buffer and re-suspended in NEB buffer (20 mM HEPES (pH 7.5), 400 mM NaCl, 1 mM EDTA, 1 mM DTT, 1 mM PMSF, 1× protease inhibitor; 25 µl per 1×10^6 cells), followed by 30-min incubation on ice. Next, the nuclei were centrifuged at 5,000*g* (4 °C), and the supernatant containing the soluble nuclear fraction was collected. The resulting cell pellet was washed again in

NEB buffer, re-supended in CEB buffer (NEB buffer, 5 mM $CaCl_2$, 150 U of MNase/1 × 10^6 cells; 25 µl per 1 × 10^6 cells) and incubated for 10 min at 37 °C to obtain the chromatin-bound fraction.

After separation via SDS-PAGE, proteins were transferred to nitrocellulose membranes (GE Healthcare, 10600002), blocked in 5% skim milk in PBST (0.1% Tween 20 in PBS) and incubated with the appropriate primary antibody followed by incubation with HRP-coupled secondary antibodies as indicated in Extended Data Table 1. Images were taken with an Amersham Imager 600 (GE Healthcare Life Sciences).

RNA isolation, RT–PCR and real-time PCR

RNA was isolated using TRIzol RNA isolation reagent (Invitrogen, 15596018). For real-time PCR analysis, cDNA was synthesized with a High Capacity cDNA Reverse Transcription Kit (Applied Biosystems, 4368813). Real-time PCR was performed using SYBR Green PCR Master Mix (Applied Biosystems, A25742) or qPCRBIO SyGreen Blue Hi-ROX (Nippon Genetics). Cycle numbers were normalized to those of α-tubulin (Tuba1a). Primers used for qPCR analysis are listed in Extended Data Table 2.

RNA-seq

P7 retinas were dissected and digested with a collagenase enzyme solution (1 mg ml^{-1} Collagenase I (Worthington, LS004196), 0.1 mg ml^{-1} DNAse I (Merck, 10104159001) in HBSS) for 1 h at 37 °C followed by filtering the cell suspension through a 70-µm cell strainer with basal medium (DMEM high glucose, 20% FBS, 1× penicillin–streptomycin, 1× L-glutamin, 25 mM HEPES). After centrifugation and washing, cells were stained with a CD31-APC coupled antibody for 30 min and sorted with a BD FACSAria IIu (BD Biosciences) for living, CD31-positive cells. Total RNA was isolated using an RNeasy Universal Mini Kit (Qiagen, 73404). The integrity of the RNA was assessed on a Bioanalyzer 2100 (Agilent) using an RNA 6000 Pico Kit (Agilent, 5067-1513). Low-input RNA library preparation (smart-seq2) and sequencing were performed on a BGISEQ-500 platform.

For RNA-seq of control and *RNF20*-deficient HUVECs, total RNA of siRNA-transfected HUVECs was isolated 60 h after transfection using the RNeasy Universal Mini Kit. The RNA integrity was assessed on a Bioanalyzer 2100 using an RNA 6000 Nano Kit (Agilent, 5067-1511), and standard library preparation and sequencing were performed on a BGISEQ-500 platform.

RNA-seq data analysis

RNA-seq reads were trimmed of adapters using Trimmomatic (version 0.39) and mapped to the mm10 reference genome using STAR[56] (version 2.7.3a) (–alignIntronMin 20 –alignIntronMax 500000). Read quality was controlled by the MultiQC tool (version 1.14), and reads were counted using the analyzeRepeats.pl function (rna mm10 –count exons –strand both –noadj) from HOMER (version 4.11.1) after creating the tag directories with makeTagDirectory. Differential expression was quantified and normalized using DESeq2 (version 1.40.0). Reads per kilobase per million mapped reads (RPKM) was determined using rpkm. default from EdgeR (version 3.42.4). Differentially regulated genes were filtered as follows (retinal EC: $\log_2$ fold change ≤ −1, ≥1; $P < 0.05$; HUVECs: $\log_2$ fold change ≤ −0.58, ≥0.58; $P < 0.05$). GO and pathway analysis were performed using Metascape (version 3.5)[57]. Heatmaps were created using d3Heatmap (version 0.9.0) (http://heatmapper.ca/expression/). All heatmaps represent the row-based z-scores calculated from trimmed mean of M-values (TMM). The principal component analysis (PCA) plots were obtained using prcomp function from the stats package into a custom R script (version 4.3.0), and volcano plots were obtained using the EnhancedVolcano R package (version 1.18.0). All data, including publicly available data, were normalized with the same parameters.

Differential spliced genes were detected by using the DEXSeq[58] R package (version 1.40.0) with $P < 0.05$ and $\log_2$ fold change ≤ −1, ≥1.

ATAC-seq and data analysis

At P7, mice were euthanized and retina were dissected, followed by digestion with enzyme solution (1 mg ml^{-1} Collagenase I (Worthington, LS004196), 0.1 mg ml^{-1} DNAse I (Merck, 10104159001) in HBSS) for 45 min at 37 °C with agitation. The digestion was stopped by adding basal medium (DMEM high glucose, 20% FBS, 1× penicillin–streptomycin, 1× L-glutamin, 25 mM HEPES) and filtering the cell suspension through a 70-µm cell strainer. After centrifugation, the cell pellet was resuspended in 1 ml of basal medium and bound with CD31-coupled magnetic Dynabeads (Thermo Fisher Scientific, 11035) for 30 min at room temperature with agitation. After five washes, ECs were counted, and 5,000 cells were used for ATAC-seq protocol as described in ref. 59 with the following modifications. For 5,000 cells, the amount of the Tn5 enzyme from the Illumina tagmentation kit (cat. no. 20034211) was scaled down to 1 µl per 50-µl reaction.

ATAC-seq raw reads processing, mapping and peak calling were done according to the ENCODE ATAC-seq pipeline. Differential ATAC peaks were detected using the Diffbind R package[31] (version 3.4.11). Differentially ATAC peaks were filtered as follows ($\log_2$ fold change ≤ −0.58, ≥0.58; $P < 0.05$). Footprinting and TF network analysis were done using the TOBIAS footprinting package[31] (version 0.14.0), and the results were plotted using the EnhancedVolcano R package (version 1.18.0). TF network analysis was performed with Cytoscape (version 3.6.1) on STAT3, ERG and Fosl2 target gene networks detected in the footprinting analysis, which showed increased binding score ($\log_2$ fold change > 0.58), upregulation and involvement in the angiogenesis-related pathways.

ChIP and ChIP-seq

For H2Bub ChIP, 500,000 control and *RNF20* siRNA-transfected HUVECs were harvested and fixed for 10 min in 1% formaldehyde per each replicate. Fixation was stopped by adding glycine to a final concentration of 0.125 M. Cells were then washed twice in cold PBS and lysed in Lysis Buffer I (10 mM Tris HCl (pH 8.0), 10 mM NaCl, 0.5% NP-40) (50 µl per 500,000 cells) for 15 min at 4 °C while rotating.

For ChIP of RNA Pol II, ERG and NICD, siRNA-transfected HUVEC cells in one full six-well plate were fixed on the plate per each replicate. Fixation was performed for 10 min in 1% formaldehyde with gentle rotation at room temperature and then stopped by adding 0.125 M glycine for 5 min, followed by three washes with ice-cold PBS. Cells were harvested in Lysis Buffer I (10 mM Tris (pH 8.0), 10 mM NaCl, 0,5% NP-40, 1× protease inhibitor, 1× phosphatase inhibitor) and harvested by scraping.

For all ChIP samples, nuclei were spun down at 2,500*g* for 5 min and resuspended in Lysis Buffer II (50 mM Tris (pH 8.0), 10 mM EDTA, 0,5% SDS, 1× protease inhibitor, 1× phosphatase inhibitor) at a concentration of 1 million cells per 40 µl. Chromatin was sheared with Covaris in Lysis Buffer II containing 0.1% SDS to obtain fragments between 200 bp and 400 bp. After centrifugation at 16,000*g* for 15 min, the supernatant was transferred into a new tube and diluted with the same volume of 2× immunoprecipitation (IP) buffer (100 mM Tris (pH 8.0), 2 mM EDTA, 300 mM NaCl, 2% Triton X-100, 0.2% SDS, 0.2% sodium deoxycholate monohydrate, 1× protease inhibitor, 1× phosphatase inhibitor). The samples were pre-cleared with 100 µl of Sepharose Fast Flow 4 beads for 1.5 h at 4 °C under gentle rotation and incubated with 1 µg of total Pol II (Rpb1 NTD, 14958S, Cell Signaling Technology; 1 µg/IP), 0.5 µg of H2Bub1 (5546, Cell Signaling Technology; 0.5 µg/IP), 1 µg of ERG (ab92513, Abcam; 1 µg/IP) or 1 µg of NICD (4147, Cell Signaling Technology; 1 µg/IP) overnight at 4 °C with rotation. The next day, 50 µl of Sepharose Fast Flow 4 beads were added and incubated for two additional hours at 4 °C. The samples were then washed two times with low-salt buffer (20 mM Tris (pH 8.0), 2 mM EDTA, 150 mM NaCl, 1% Triton X-100, 0.1% SDS, 1× protease inhibitor, 1× phosphatase inhibitor), one time with high-salt buffer (20 mM Tris (pH 8.0), 2 mM EDTA, 500 mM NaCl, 1% Triton X-100, 0.1% SDS, 1× protease inhibitor, 1× phosphatase inhibitor),

one time with LiCl wash buffer (10 mM Tris (pH 8.0), 1 mM EDTA, 250 mM LiCl, 1% NP40, 1% sodium deoxycholate monohydrate, 1× protease inhibitor, 1× phosphatase inhibitor) and two times with TE buffer (10 mM Tris (pH 8.0), 1 mM EDTA, 1× protease inhibitor, 1× phosphatase inhibitor). Samples were eluted in 200 µl of elution buffer (0.6% SDS, 10 mM Tris (pH 8.0), 0.5 mM EDTA, 300 mM NaCl) and treated with RNase A, followed by proteinase K treatment and reverse crosslinking overnight at 65 °C. The DNA was purified with a Zymo kit (D5205).

For ChIP–qPCR, 0.1 ng of DNA was used per reaction.

For ChIP-seq, libraries were prepared with a NEBNext Ultra II DNA Library Prep Kit for Illumina (New England Biolabs, E7645S/L and E7103S/L) according to the manufacturer's instructions.

ChIP-seq data analysis

ChIP-seq reads were trimmed using Trimmomatic (version 0.39), minimum length of 60 bp and a quality score of a minimum of 15. Trimmed reads were mapped to mouse genome mm10 (UCSC assembly) with using Bowtie2 (version 2.4.4) (default settings). SAMtools view (version 1.7.) was used to convert SAM files to BAM format. PCR artifacts were removed by the MarkDuplicates.jar function from Picard (version 1.119). Individual BAM-mapped files were merged using BamTools (version 2.5.1) merge (default settings). Merged BAM files were converted to BigWig format using BamCoverage from deepTools (version 3.5.1) (-b 20 -smooth 40 --normalizeUsing RPKM -e 150). Peaks were called using MACS2 (version 2.2.7.1) (callpeak, --broad --nomodel -g mmu -p 0.01 --shift −75 --extsize 150 --keep-dup all). Peaks overlapping the blacklist defined by ENCODE were removed. ERG-ChIP-seq enrichment of Rnf20 deregulated genes was performed using plotProfile from deepTools. ngs.plot (version 2.41.4) was used to plot the H2Bub-ChIP-seq enrichment genome wide and at Notch targets.

Calculation of PI from Pol II ChIP-seq data

PI was calculated by dividing the normalized count per million reads on the TSS area (−50 bp to 300 bp) by those on the gene body plus 3 kb after the TTS. For the calculation, the GitHub repository code (https://github.com/MiMiroot/PIC) was used with settings (--gtf hg38.gtf --TSSup 50 --TSSdown 300 --GBdown 3000) and Ensembl hg38, version 108. Highly paused genes were defined as the genes with PI > quartile 3 (Q3) in the control samples. *P* values were calculated using the Wilcoxon test from the library (rstatix) (version 0.7.2) from the R language.

To calculate differential pausing, we used the *t*-test function from the rstatix package on PI values from replicates of control and siRNF20 or ERG-overexpressing HUVECs. Genes with decreased PI were identified as those with a $\log_2$ PI < 0.5 and a false discovery rate (FDR) < 0.25. All scripts for processing the pausing matrices are available in the repository at https://github.com/jcorderJC12/02PAUSING_P2t.

Statistics and reproducibility

All experiments were performed at least three independent times in biological replicates, and the respective data were used for statistical analyses.

For animal experiments, mice (C57BL/6J) were grouped into control (C57BL/6_*PdgfbiCre2*^{neg}_*Rnf20tm1c(EUCOMM)Wtsi*$^{flox/flox}$) and *Rnf20*^{iECKO} (C57BL/6_*PdgfbiCre2*^{pos}_*Rnf20tm1c(EUCOMM)Wtsi*$^{flox/flox}$) cohorts, irrespective of their sex. The data presented were obtained from retinas isolated from individual mice. Quantifications in Figs. 1d,f,h,j,l,n,p,s and 7h,i and Extended Data Figs. 1e,f,h,i,j and 6f,h were performed on mice at P7, whereas quantifications in Fig. 2f were conducted on mice at P28. Differences between groups were assessed using an unpaired two-tailed Student's *t*-test or ANOVA multiple comparisons test as indicated in the figure legends. For all tests, $P < 0.05$ was considered statistically significant. Bar plots and box plots were produced with GraphPad Prism 10 software. Numeric *P* values are shown within the figures.

Reporting summary

Further information on research design is available in the Nature Portfolio Reporting Summary linked to this article.

Data availability

Sequencing data generated in this study have been deposited in the Gene Expression Omnibus (accession number GSE212524). Processed data are included in the source data for each figure. Single-cell data from neonatal mouse retinas (GSE175895), ChIP-seq of ERG (GSE124893) and ETS1 (GSM2442778) in HUVECs were retrieved from previously published studies. Figures that have associated raw data include Figs. 3a–d,f–k, 4a–c,f, 5h,i,k and 6a–g and Extended Data Figs. 2a–g,i,j, 3a,b, 4a–d,g,h and 5a–c. Source data are provided with this paper.

References

1. Blanco, R. & Gerhardt, H. VEGF and Notch in tip and stalk cell selection. *Cold Spring Harb. Perspect. Med.* **3**, a006569 (2013).
2. Eilken, H. M. & Adams, R. H. Dynamics of endothelial cell behavior in sprouting angiogenesis. *Curr. Opin. Cell Biol.* **22**, 617–625 (2010).
3. Hasan, S. S. et al. Endothelial Notch signalling limits angiogenesis via control of artery formation. *Nat. Cell Biol.* **19**, 928–940 (2017).
4. Hellstrom, M. et al. Dll4 signalling through Notch1 regulates formation of tip cells during angiogenesis. *Nature* **445**, 776–780 (2007).
5. Jakobsson, L. et al. Endothelial cells dynamically compete for the tip cell position during angiogenic sprouting. *Nat. Cell Biol.* **12**, 943–953 (2010).
6. Lee, H. W. et al. Role of venous endothelial cells in developmental and pathologic angiogenesis. *Circulation* **144**, 1308–1322 (2021).
7. Pitulescu, M. E. et al. Dll4 and Notch signalling couples sprouting angiogenesis and artery formation. *Nat. Cell Biol.* **19**, 915–927 (2017).
8. Pontes-Quero, S. et al. High mitogenic stimulation arrests angiogenesis. *Nat. Commun.* **10**, 2016 (2019).
9. Potente, M. & Makinen, T. Vascular heterogeneity and specialization in development and disease. *Nat. Rev. Mol. Cell Biol.* **18**, 477–494 (2017).
10. Stewen, J. et al. Eph-ephrin signaling couples endothelial cell sorting and arterial specification. *Nat. Commun.* **15**, 2539 (2024).
11. Xu, C. et al. Arteries are formed by vein-derived endothelial tip cells. *Nat. Commun.* **5**, 5758 (2014).
12. Udan, R. S., Vadakkan, T. J. & Dickinson, M. E. Dynamic responses of endothelial cells to changes in blood flow during vascular remodeling of the mouse yolk sac. *Development* **140**, 4041–4050 (2013).
13. Hargreaves, D. C., Horng, T. & Medzhitov, R. Control of inducible gene expression by signal-dependent transcriptional elongation. *Cell* **138**, 129–145 (2009).
14. Levine, M. Paused RNA polymerase II as a developmental checkpoint. *Cell* **145**, 502–511 (2011).
15. Liu, X., Kraus, W. L. & Bai, X. Ready, pause, go: regulation of RNA polymerase II pausing and release by cellular signaling pathways. *Trends Biochem. Sci.* **40**, 516–525 (2015).
16. Adelman, K. & Lis, J. T. Promoter-proximal pausing of RNA polymerase II: emerging roles in metazoans. *Nat. Rev. Genet.* **13**, 720–731 (2012).
17. Galbraith, M. D. et al. HIF1A employs CDK8-mediator to stimulate RNAPII elongation in response to hypoxia. *Cell* **153**, 1327–1339 (2013).
18. Day, D. S. et al. Comprehensive analysis of promoter-proximal RNA polymerase II pausing across mammalian cell types. *Genome Biol.* **17**, 120 (2016).
19. Kim, J. et al. RAD6-mediated transcription-coupled H2B ubiquitylation directly stimulates H3K4 methylation in human cells. *Cell* **137**, 459–471 (2009).

20. Kim, J., Hake, S. B. & Roeder, R. G. The human homolog of yeast BRE1 functions as a transcriptional coactivator through direct activator interactions. *Mol. Cell* **20**, 759–770 (2005).
21. Pavri, R. et al. Histone H2B monoubiquitination functions cooperatively with FACT to regulate elongation by RNA polymerase II. *Cell* **125**, 703–717 (2006).
22. Shema, E., Kim, J., Roeder, R. G. & Oren, M. RNF20 inhibits TFIIS-facilitated transcriptional elongation to suppress pro-oncogenic gene expression. *Mol. Cell* **42**, 477–488 (2011).
23. Zaidi, S. et al. De novo mutations in histone-modifying genes in congenital heart disease. *Nature* **498**, 220–223 (2013).
24. Zhang, M. et al. Endothelial cells regulated by RNF20 orchestrate the proliferation and differentiation of neural precursor cells during embryonic development. *Cell Rep.* **40**, 111350 (2022).
25. Zarkada, G. et al. Specialized endothelial tip cells guide neuroretina vascularization and blood-retina-barrier formation. *Dev. Cell* **56**, 2237–2251 (2021).
26. del Toro, R. et al. Identification and functional analysis of endothelial tip cell-enriched genes. *Blood* **116**, 4025–4033 (2010).
27. Brash, J. T. et al. Tamoxifen-activated CreERT impairs retinal angiogenesis independently of gene deletion. *Circ. Res.* **127**, 849–850 (2020).
28. Bentley, D. L. Coupling mRNA processing with transcription in time and space. *Nat. Rev. Genet.* **15**, 163–175 (2014).
29. Moyal, L. et al. Requirement of ATM-dependent monoubiquitylation of histone H2B for timely repair of DNA double-strand breaks. *Mol. Cell* **41**, 529–542 (2011).
30. Nakamura, K. et al. Regulation of homologous recombination by RNF20-dependent H2B ubiquitination. *Mol. Cell* **41**, 515–528 (2011).
31. Bentsen, M. et al. ATAC-seq footprinting unravels kinetics of transcription factor binding during zygotic genome activation. *Nat. Commun.* **11**, 4267 (2020).
32. Bray, S., Musisi, H. & Bienz, M. Bre1 is required for Notch signaling and histone modification. *Dev. Cell* **8**, 279–286 (2005).
33. Birdsey, G. M. et al. The endothelial transcription factor ERG promotes vascular stability and growth through Wnt/β-catenin signaling. *Dev. Cell* **32**, 82–96 (2015).
34. Kalna, V. et al. The transcription factor ERG regulates super-enhancers associated with an endothelial-specific gene expression program. *Circ. Res.* **124**, 1337–1349 (2019).
35. Shah, A. V. et al. The endothelial transcription factor ERG mediates Angiopoietin-1-dependent control of Notch signalling and vascular stability. *Nat. Commun.* **8**, 16002 (2017).
36. Fish, J. E. et al. Dynamic regulation of VEGF-inducible genes by an ERK/ERG/p300 transcriptional network. *Development* **144**, 2428–2444 (2017).
37. Sissaoui, S. et al. Genomic characterization of endothelial enhancers reveals a multifunctional role for NR2F2 in regulation of arteriovenous gene expression. *Circ. Res.* **126**, 875–888 (2020).
38. Chen, J. et al. VEGF amplifies transcription through ETS1 acetylation to enable angiogenesis. *Nat. Commun.* **8**, 383 (2017).
39. Muniz, L., Nicolas, E. & Trouche, D. RNA polymerase II speed: a key player in controlling and adapting transcriptome composition. *EMBO J.* **40**, e105740 (2021).
40. Fuchs, G., Hollander, D., Voichek, Y., Ast, G. & Oren, M. Cotranscriptional histone H2B monoubiquitylation is tightly coupled with RNA polymerase II elongation rate. *Genome Res.* **24**, 1572–1583 (2014).
41. Mineur, P. et al. Newly identified biologically active and proteolysis-resistant VEGF-A isoform VEGF111 is induced by genotoxic agents. *J. Cell Biol.* **179**, 1261–1273 (2007).
42. Olsson, A. K., Dimberg, A., Kreuger, J. & Claesson-Welsh, L. VEGF receptor signalling—in control of vascular function. *Nat. Rev. Mol. Cell Biol.* **7**, 359–371 (2006).
43. Simons, M., Gordon, E. & Claesson-Welsh, L. Mechanisms and regulation of endothelial VEGF receptor signalling. *Nat. Rev. Mol. Cell Biol.* **17**, 611–625 (2016).
44. Munoz, M. J. et al. DNA damage regulates alternative splicing through inhibition of RNA polymerase II elongation. *Cell* **137**, 708–720 (2009).
45. Delcombel, R. et al. New prospects in the roles of the C-terminal domains of VEGF-A and their cooperation for ligand binding, cellular signaling and vessels formation. *Angiogenesis* **16**, 353–371 (2013).
46. Ong, C. T. & Corces, V. G. Enhancer function: new insights into the regulation of tissue-specific gene expression. *Nat. Rev. Genet.* **12**, 283–293 (2011).
47. Krebs, L. T., Deftos, M. L., Bevan, M. J. & Gridley, T. The *Nrarp* gene encodes an ankyrin-repeat protein that is transcriptionally regulated by the Notch signaling pathway. *Dev. Biol.* **238**, 110–119 (2001).
48. Lamar, E. et al. Nrarp is a novel intracellular component of the Notch signaling pathway. *Genes Dev.* **15**, 1885–1899 (2001).
49. Phng, L. K. et al. Nrarp coordinates endothelial Notch and Wnt signaling to control vessel density in angiogenesis. *Dev. Cell* **16**, 70–82 (2009).
50. Fischer, A. & Gessler, M. Delta–Notch—and then? Protein interactions and proposed modes of repression by Hes and Hey bHLH factors. *Nucleic Acids Res.* **35**, 4583–4596 (2007).
51. Nakayama, M. et al. Spatial regulation of VEGF receptor endocytosis in angiogenesis. *Nat. Cell Biol.* **15**, 249–260 (2013).
52. Sethi, G., Shanmugam, M. K., Arfuso, F. & Kumar, A. P. Role of RNF20 in cancer development and progression - a comprehensive review. *Biosci. Rep.* **38**, BSR20171287 (2018).
53. Claxton, S. et al. Efficient, inducible Cre-recombinase activation in vascular endothelium. *Genesis* **46**, 74–80 (2008).
54. Pitulescu, M. E., Schmidt, I., Benedito, R. & Adams, R. H. Inducible gene targeting in the neonatal vasculature and analysis of retinal angiogenesis in mice. *Nat. Protoc.* **5**, 1518–1534 (2010).
55. Heiss, M. et al. Endothelial cell spheroids as a versatile tool to study angiogenesis in vitro. *FASEB J.* **29**, 3076–3084 (2015).
56. Dobin, A. et al. STAR: ultrafast universal RNA-seq aligner. *Bioinformatics* **29**, 15–21 (2013).
57. Zhou, Y. et al. Metascape provides a biologist-oriented resource for the analysis of systems-level datasets. *Nat. Commun.* **10**, 1523 (2019).
58. Anders, S., Reyes, A. & Huber, W. Detecting differential usage of exons from RNA-seq data. *Genome Res.* **22**, 2008–2017 (2012).
59. Buenrostro, J. D., Wu, B., Chang, H. Y. & Greenleaf, W. J. ATAC-seq: a method for assaying chromatin accessibility genome-wide. *Curr. Protoc. Mol. Biol.* **109**, 21.29.21–21.29.29 (2015).

Acknowledgements

We would like to thank S. Uhlig, the FlowCore Mannheim and the Core Facility Preclinical Models for excellent support. G.D. was supported by the Collaborative Research Center 1366 (project A03), funded by the German Research Foundation (DFG); the German Centre for Cardiovascular Research (DZHK) (81Z0500202 and 81X2500216), funded by the Federal Ministry of Education and Research (BMBF); and the Baden-Württemberg Foundation special program 'Angioformatics Single Cell Platform'. M.P. was supported by a European Research Council Consolidator Grant (EMERGE-773047), the DFG (project number 456687919 – SFB 1531) and a Leducq Foundation grant.

Author contributions

N.T.-E., A.E., A.S., J.G., Y.T. and P.G. performed the experiments. N.T.-E., A.E., A.D., Y.D. and J.C. performed the bioinformatic analysis. M.P., A.D., H.S., T.W. and J.H. provided reagents and valuable intellectual input. N.T.-E., J.C., R.O. and G.D. designed the experiments, analyzed the data and wrote the paper. All authors discussed the results and commented on the paper.

Competing interests
The authors declare no competing interests.

Additional information
Extended data is available for this paper at https://doi.org/10.1038/s44161-024-00546-5.

Supplementary information The online version contains supplementary material available at https://doi.org/10.1038/s44161-024-00546-5.

Correspondence and requests for materials should be addressed to Julio Cordero, Roxana Ola or Gergana Dobreva.

Peer review information *Nature Cardiovascular Research* thanks the anonymous reviewer(s) for their contribution to the peer review of this work.

Reprints and permissions information is available at www.nature.com/reprints.

[1]Department of Cardiovascular Genomics and Epigenomics, European Center for Angioscience (ECAS), Medical Faculty Mannheim, Heidelberg University, Mannheim, Germany. [2]Cardiovascular Pharmacology, European Center for Angioscience, Medical Faculty Mannheim, Heidelberg University, Mannheim, Germany. [3]German Centre for Cardiovascular Research (DZHK), Mannheim, Germany. [4]Experimental Pharmacology, European Center for Angioscience (ECAS), Medical Faculty Mannheim, Heidelberg University, Mannheim, Germany. [5]Centre de Recherche, CHU St. Justine, Montreal, Quebec, Canada. [6]Department of Cardiovascular Physiology, European Center for Angioscience (ECAS), Medical Faculty Mannheim, Heidelberg University, Mannheim, Germany. [7]Angiogenesis & Metabolism Laboratory, Center of Vascular Biomedicine, Berlin Institute of Health at Charité—Universitätsmedizin Berlin, Berlin, Germany. [8]Max Delbrück Center for Molecular Medicine in the Helmholtz Association, Berlin, Germany. [9]Helmholtz-Institute for Translational AngioCardioScience (HI-TAC) of the Max Delbrück Center for Molecular Medicine in the Helmholtz Association (MDC) at Heidelberg University, Heidelberg, Germany. ✉e-mail: julio.cordero@medma.uni-heidelberg.de; roxana.ola@medma.uni-heidelberg.de; gergana.dobreva@medma.uni-heidelberg.de

https://doi.org/10.1038/s44161-024-00546-5

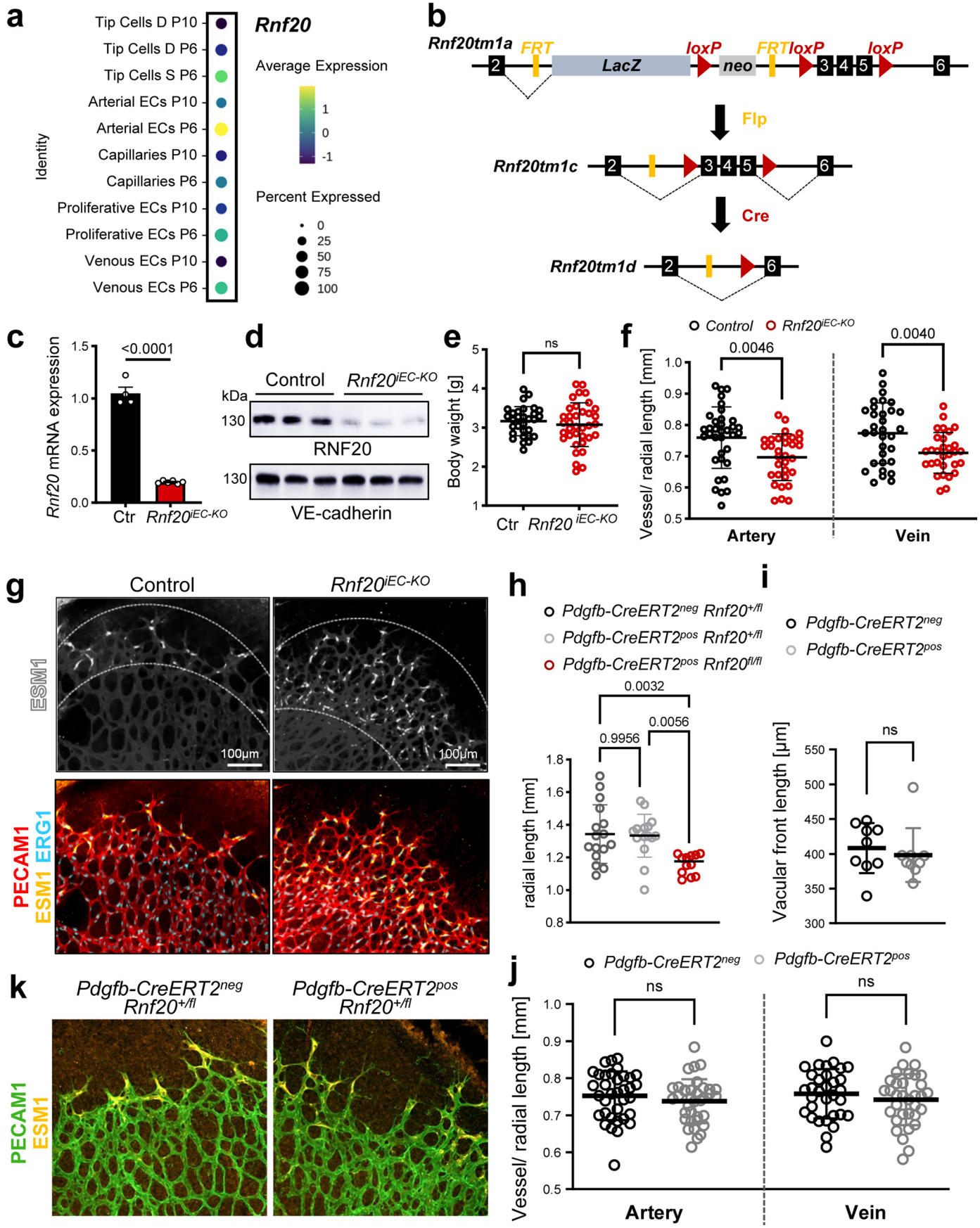

Extended Data Fig. 1 | See next page for caption.

https://doi.org/10.1038/s44161-024-00546-5

Extended Data Fig. 1 | Role of RNF20 in retinal vessel growth and patterning. **a** Dot plot of *Rnf20* expression level and frequency in EC from P6 and P10 retinas[25]. **b** Schematic diagram of the *Rnf20* targeting construct and the crosses used for the generation of inducible (floxed) allele in ECs. **c, d** mRNA expression of *Rnf20* (**c**) and WB using anti-RNF20 antibody and VE-cadherin (Cdh5) as an EC loading control (**d**) of ECs isolated from lungs of control and $Rnf20^{iEC\text{-}KO}$ mice. n = 4 Control; n = 6 $Rnf20^{iEC\text{-}KO}$. **e** Body weight of control and $Rnf20^{iEC\text{-}KO}$ mice. Dots represent individual pups (n = 30 control, n = 36 $Rnf20^{iECKO}$). **f** Quantification of vessel length normalized to radial length (µm); n = 10 control and 10 $Rnf20^{iEC\text{-}KO}$ retinas; n = 35 Control arteries, n = 32 $Rnf20^{iEC\text{-}KO}$ arteries, n = 32 Control veins; n = 30 $Rnf20^{iEC\text{-}KO}$ veins. **g** Immunostaining for ESM1, ERG and CD31 showing excessive tip cell formation in $Rnf20^{iEC\text{-}KO}$. **h** Quantification of the radial length in $Pdgfb\text{-}CreERT2^{neg}Rnf20^{+/fl}$ (n = 4); $Pdgfb\text{-}CreERT2^{pos}Rnf20^{+/fl}$ (n = 4) and $Pdgfb\text{-}CreERT2^{pos}Rnf20^{fl/fl}$ (n = 3) retinas; each data point represents one leaflet. **i** Quantification of the length of the vascular front in $Pdgfb\text{-}CreERT2^{neg}$ and $Pdgfb\text{-}CreERT2^{pos}$ retinas (n = 9 for each group). **j** Quantification of the length of arteries and veins normalized to radial length in $Pdgfb\text{-}CreERT2^{neg}$ and $Pdgfb\text{-}CreERT2^{pos}$ retinas (each data point represents one leaflet of n = 8 retinas for each group). **k** Immunostaining for ESM1 and Pecam1 of $Pdgfb\text{-}CreERT2^{neg}$ and $Pdgfb\text{-}CreERT2^{pos}$ retinas. Data in e, f, i and j represent mean ± SEM; differences between groups were assessed using an unpaired two-tailed Student's t-test. Data in h represent mean ± SEM; differences between groups were assessed using one-way ANOVA multiple comparisons test. ns: not significant. Numeric p-values are shown within the figures.

https://doi.org/10.1038/s44161-024-00546-5

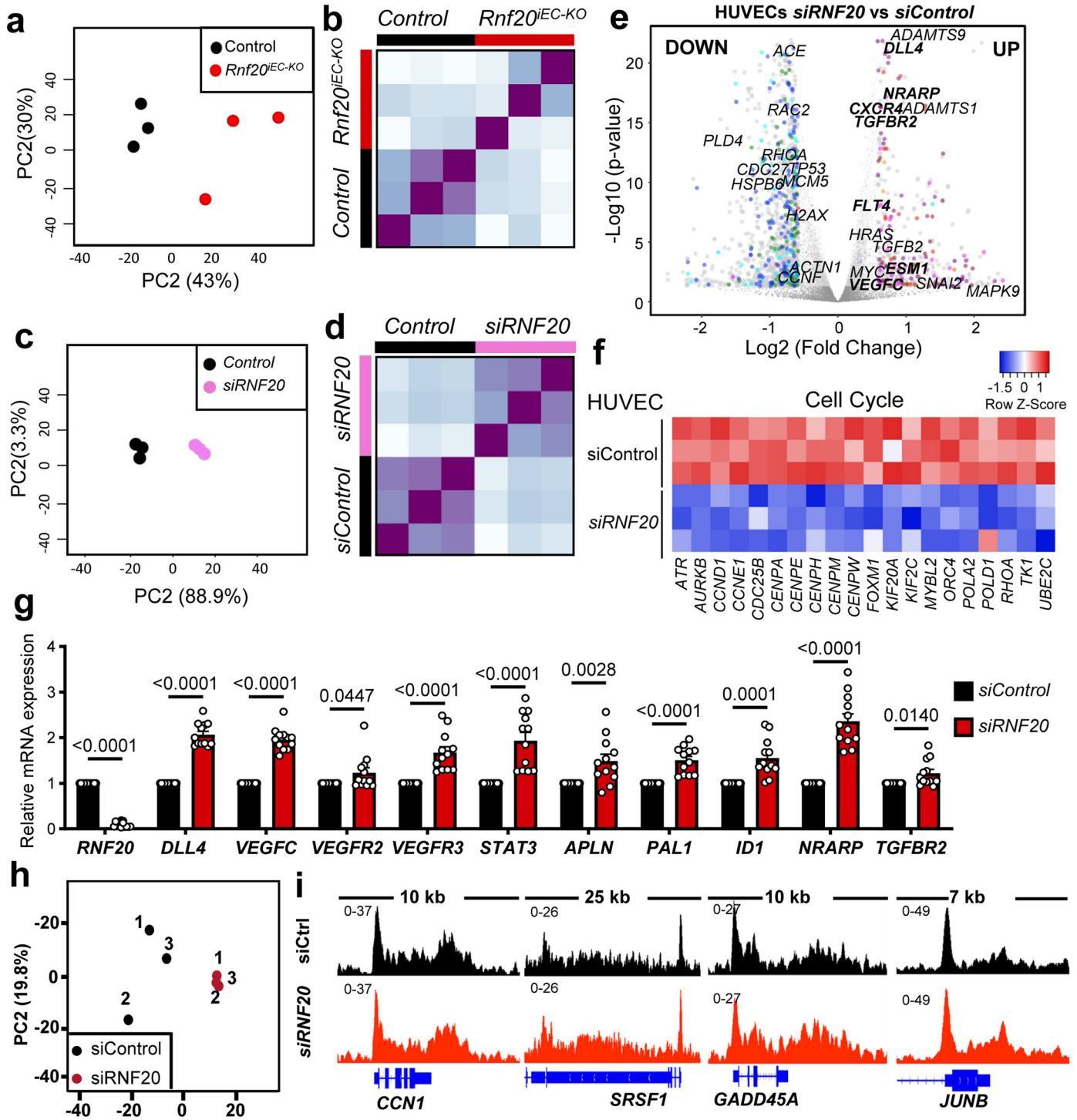

Extended Data Fig. 2 | Transcriptional changes in mouse retinal ECs and HUVECs upon RNF20 loss. a Principal component analysis (PCA) of genome-wide gene expression variation of sorted control and *Rnf20*$^{iEC-KO}$ retinal ECs (n = 3). **b** Correlation heatmap of RPKM normalized RNA-seq reads in control and *Rnf20*$^{iEC-KO}$ retinal ECs. **c** Principal component analysis (PCA) of genome-wide gene expression variation of HUVECs transfected with control or *RNF20* siRNAs for 60 h (n = 3). **d** Correlation heatmap of RPKM normalized RNA-seq reads in control and *RNF20* knockdown HUVECs. **e** Volcano plot showing the distribution of differentially expressed genes in HUVECs transfected with control and *RNF20* siRNAs. n = 3; log2 fold change ≤ −0.58, ≥0.58; p-value < 0.05. Differential expression was performed with Deseq2 (v1.40.1). **f** Heatmap representation of cell cycle related genes downregulated in HUVECs upon RNF20 loss. **g** qPCR validation of RNF20-dependent transcriptional alterations in HUVECs transfected with control and *RNF20* siRNA (n = 12). **h** Principal component analysis (PCA) of genome-wide Pol II binding variation in HUVECs transfected with control and *RNF20* siRNAs (n = 3 independent ChIP-Seq experiments). **i** Genome tracks of merged total Pol II ChIP-Seq reads at *CCN1, SRSF1, GADD45A* and *JUNB* loci. Data in g represent mean ± SEM; differences between groups were assessed using an unpaired two-tailed Student's t-test. Numeric p-values are shown within the figures.

https://doi.org/10.1038/s44161-024-00546-5

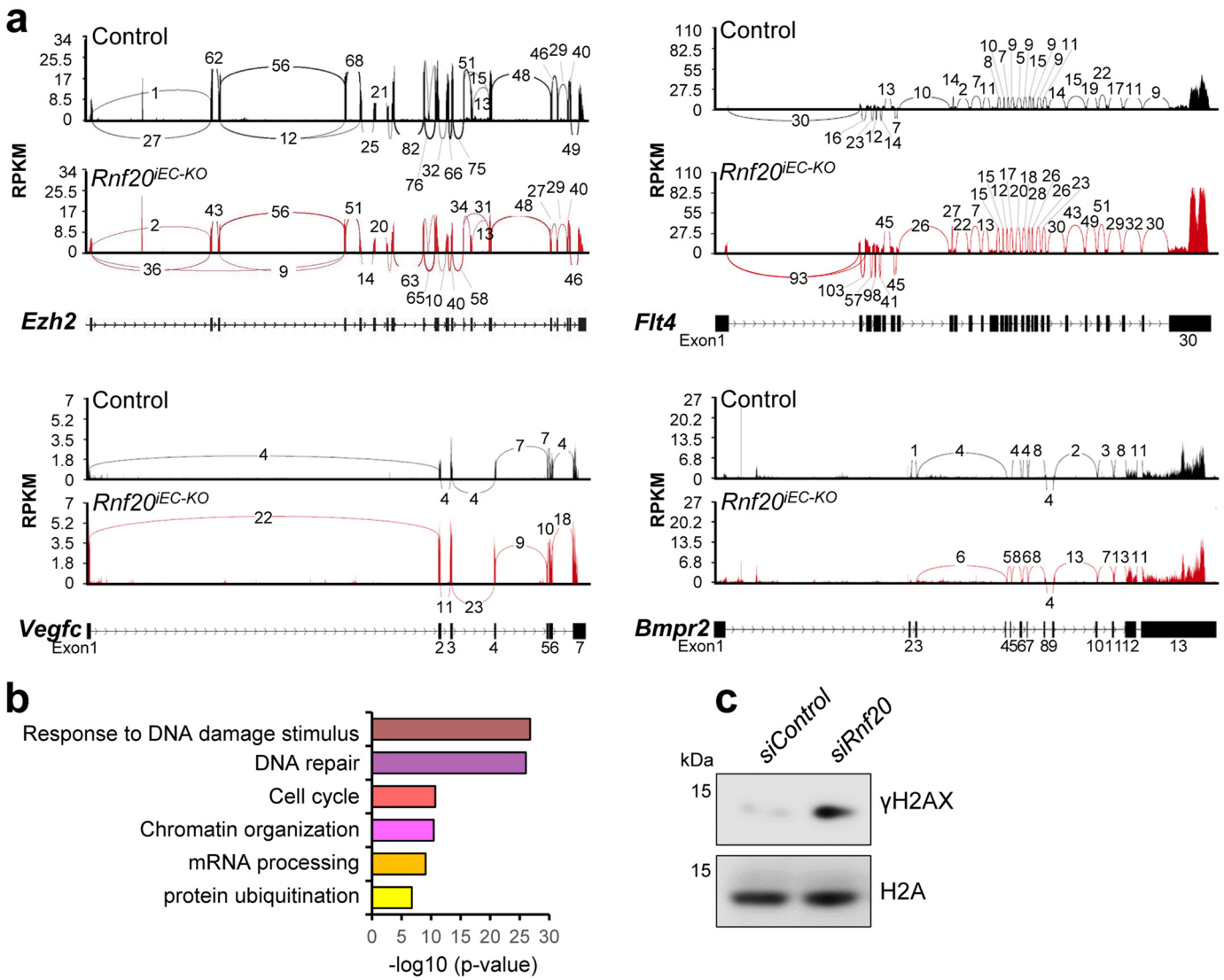

Extended Data Fig. 3 | Splicing changes in endothelial cells upon *Rnf20* loss of function. a Genome tracks of merged RNA-Seq reads at the *Ezh2*, *Vegfr3* (*Flt4*), *Vegfc* and *Bmpr2* gene loci in control and *Rnf20*$^{iEC\text{-}KO}$ retina ECs, showing alternative splicing in *Rnf20*$^{iEC\text{-}KO}$ retina ECs. **b** Top GO terms of DSG (DSG, $p \leq 0.05$, log2 fold change $\leq -1, \geq 1$, n = 3) with no change in expression levels in *Rnf20*$^{iEC\text{-}KO}$ versus control retina ECs. GO term enrichment analysis was performed on differentially spliced genes using Metascape (v.3.5). The bars represent the -log10(p-value) for each enriched GO term. **c** Western blot analysis for γH2AX, a sensitive DNA damage marker, in chromatin bound fractions from HUVECs transfected with control *siRNA* and siRNA against *RNF20*. H2A served as a loading control.

https://doi.org/10.1038/s44161-024-00546-5

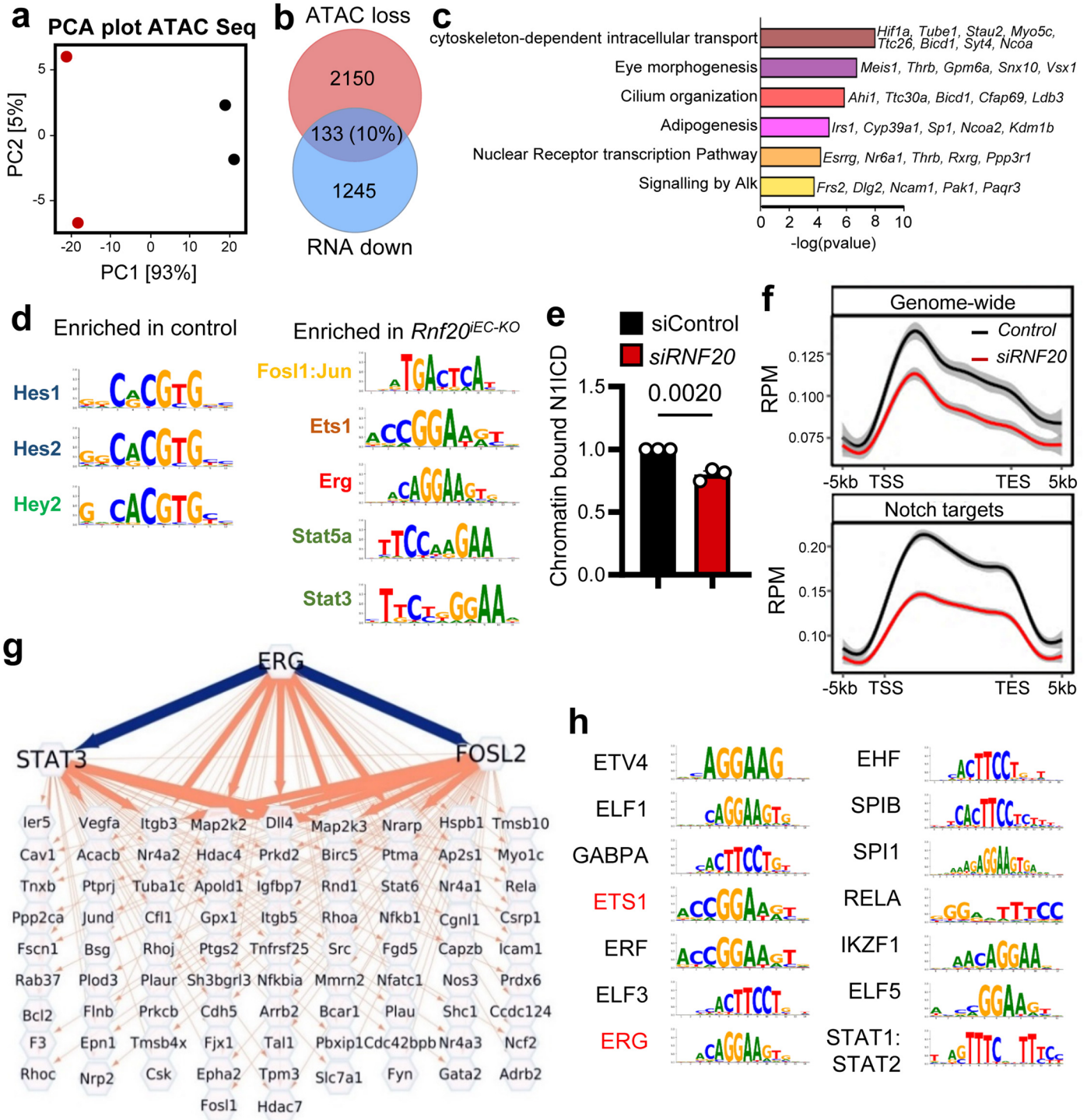

Extended Data Fig. 4 | Alterations in chromatin accessibility and transcription factor motif enrichment in RNF20-depleted ECs. a PCA of genome-wide gene chromatin accessibility variation of sorted control and *Rnf20*$^{iEC\text{-}KO}$ retina ECs (n = 2). **b, c** Venn diagram showing overlap between genes with decreased chromatin accessibility and decreased expression in *Rnf20*$^{iEC\text{-}KO}$ retinal ECs (**b**) and GO analysis of genes within the overlap (**c**). GO term enrichment analysis was performed on differentially spliced genes using Metascape (v.3.5). The bars represent the -log10(p-value) for each enriched GO term. **d** Motifs of transcription factors enriched in control (left) or in *Rnf20*$^{iEC\text{-}KO}$ retina ECs (right). **e** Quantification of N1ICD levels in three independent preparations of chromatin bound fractions of control and *RNF20* siRNA transfected HUVECs (n = 3 biological replicates for each group). H2B served as a loading control. **f** Average H2Bub1 ChIP-Seq profile genome-wide and at Notch targets in HUVECs transfected with control *siRNA* and siRNA against *RNF20*; the line plots represent mean values, with shaded areas representing the ± SEM across n = 3 biological replicates for each froup. **g** Transcription factor-gene regulatory network build on the basis of ERG, STAT3 and FOSL2 footprinting analysis. **h** Motifs of transcription factors enriched in both HUVECs transfected with *RNF20* siRNAs versus control siRNA and in *Rnf20*$^{iEC\text{-}KO}$ versus control retina ECs. Data in e represent mean ± SEM; differences between groups were assessed using an unpaired two-tailed Student's t-test.

https://doi.org/10.1038/s44161-024-00546-5

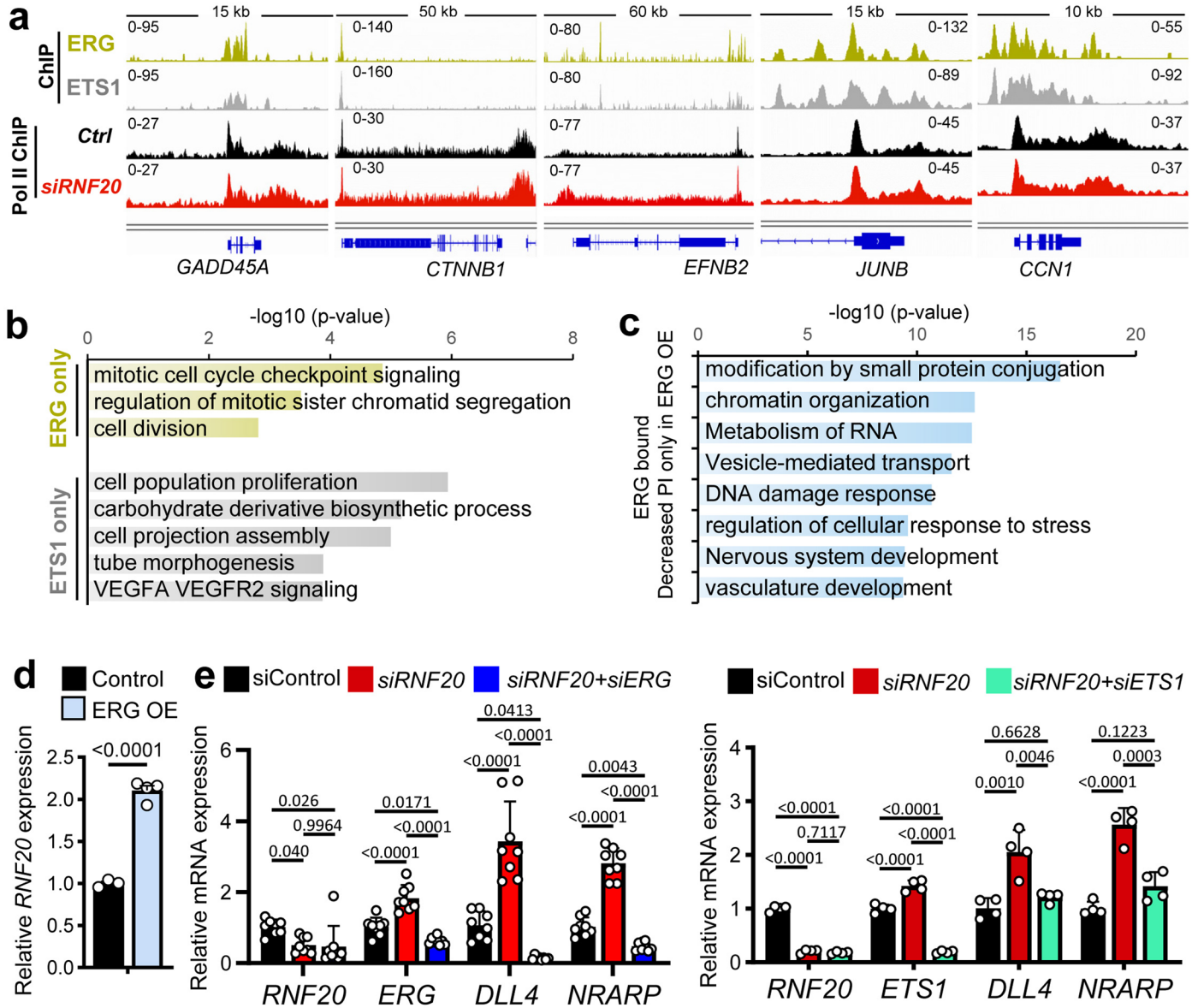

Extended Data Fig. 5 | ERG and ETS1 function in RNF20-dependent transcriptional control. a Genome tracks of ERG (light green), ETS1 (grey) ChIP-Seq reads and merged total Pol II ChIP-Seq reads (n = 3) in HUVECs transfected with control (black) or si*RNF20* (red). **b** GO analysis of genes bound only by ERG or only by ETS1 with genes showing decreased PI upon *RNF20* loss. **c** GO analysis of genes bound only by ERG with genes showing decreased PI upon ERG overexpression. **d** Relative *RNF20* mRNA levels in control and ERG OE HUVECs (n = 3 siControl n = 4 *siRNF20*). **e** qPCR for *DLL4* and *NRARP* in HUVECs transfected with control, *RNF20* siRNAs alone or together with *ERG* siRNA (left, n = 8) or HUVECs transfected with control, *RNF20* siRNAs alone or together with *ETS1* siRNA (right, n = 4 for all groups). Data in d represent mean ± SEM; differences between groups were assessed using an unpaired two-tailed Student's t-test. Data in e represent mean ± SEM; differences between groups were assessed using one-way ANOVA multiple comparisons test. GO term enrichment analysis in b and c were performed on differentially spliced genes using Metascape (v.3.5). The bars represent the -log10(p-value) for each enriched GO term. Numeric p-values are shown within the figures.

https://doi.org/10.1038/s44161-024-00546-5

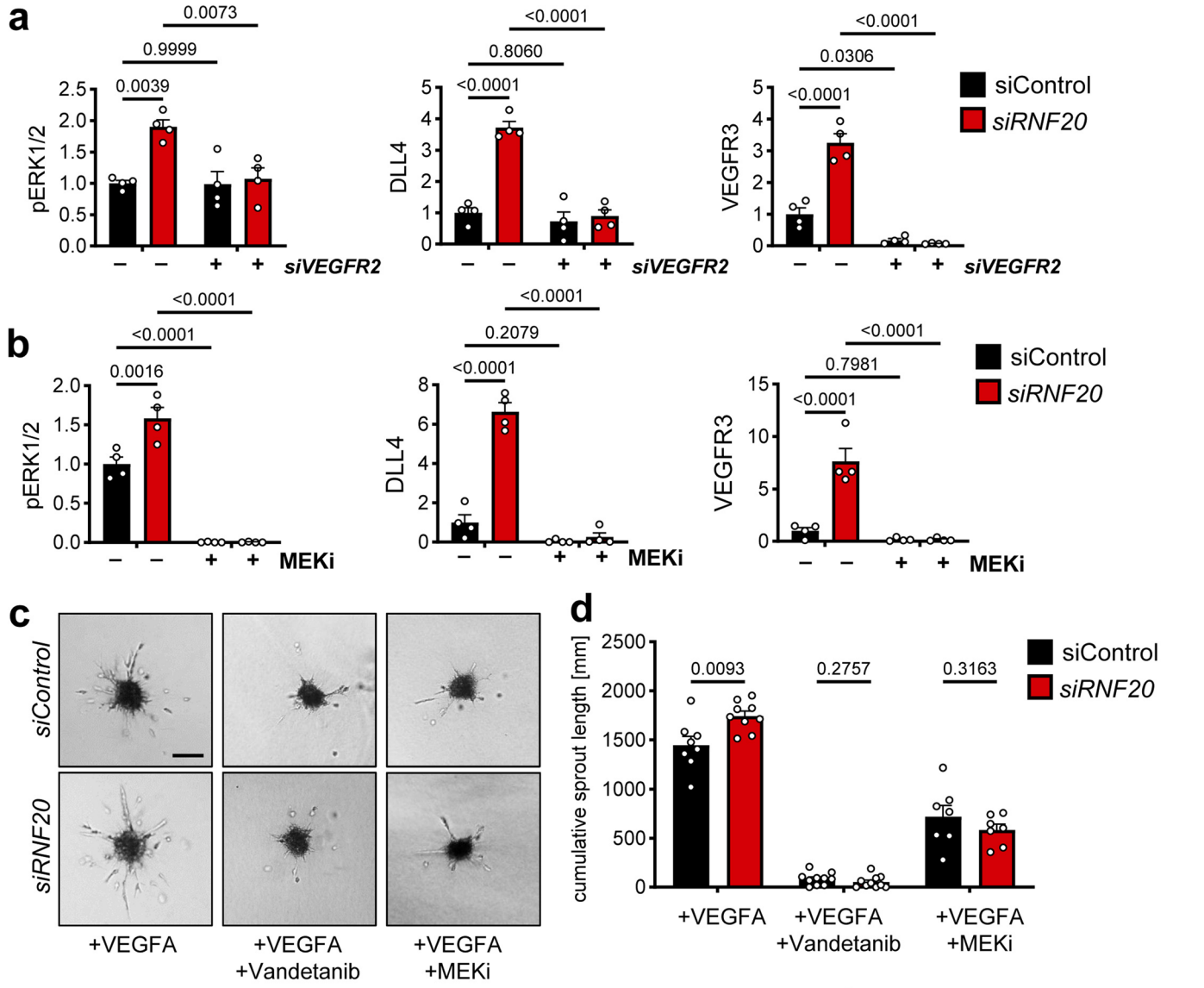

Extended Data Fig. 6 | See next page for caption.

https://doi.org/10.1038/s44161-024-00546-5

Extended Data Fig. 6 | Activation of the VEGF-ERK1/2 signaling axis upon RNF20 loss is responsible for tip cell selection. a, b WB quantification for pERK$^{Thr202/Tyr204}$, DLL4 and VEGFR3 protein levels normalized to α-tubulin of total protein extracts of HUVECs transfected with control, *VEGFR2* and *RNF20* siRNA; (**a**) or of HUVECs transfected with control or *RNF20* siRNA and either treated with DMSO or MEK inhibitor PD0325901 (**b**) for 24 h; n = 4 biological replictaes for control for each group, 4 biological replictaes for *Rnf20*$^{iEC\text{-}KO}$ for each group; figures represent mean ± SEM; statistics were quantified with two-way-ANOVA with Tukey's correction. **c, d** Sprouting assay with HUVECs transfected with control or *RNF20* siRNA and treated with DMSO, the VEGFR inhibitor Vandetanib (ZD6474) or the MEK inhibitor PD0325901 for 24 h, with VEGFA supplementation (**c**) and quantification of the cumulative sprout length (**d**). (n = 8 for siControl, n = 9 siControl+Vandetanib, n = 7 siControl + MEKI, n = 9 for *siRNF20*, n = 11 for *siRNF20*+Vandetanib, n = 7 *siRNF20* + MEKI). **e, g** Immunostaining for CD31 in control and *Rnf20*$^{iEC\text{-}KO}$ retinas treated either with PBS or DC101 (**e**) or oil and the MEK inhibitor SL327 (**g**). **f, h** Quantification of filopodia length in control and *Rnf20*$^{iEC\text{-}KO}$ retina ECs treated either with PBS or DC101 (**f**) or oil and the MEK inhibitor SL327 (**h**); each data point represents one leaflet of n = 4 control and 4 *Rnf20*$^{iEC\text{-}KO}$ retinas treated with PBS or DC101; n = 4 control+oil, 4 *Rnf20*$^{iEC\text{-}KO}$+oil, 2 control+SL327, 4 *Rnf20*$^{iEC\text{-}KO}$ + SL327 retinas (**h**); figures represent mean ± SEM; statistics were quantified with two-way-ANOVA with Tukey's correction. Numeric p-values are shown within the figures.

https://doi.org/10.1038/s44161-024-00546-5

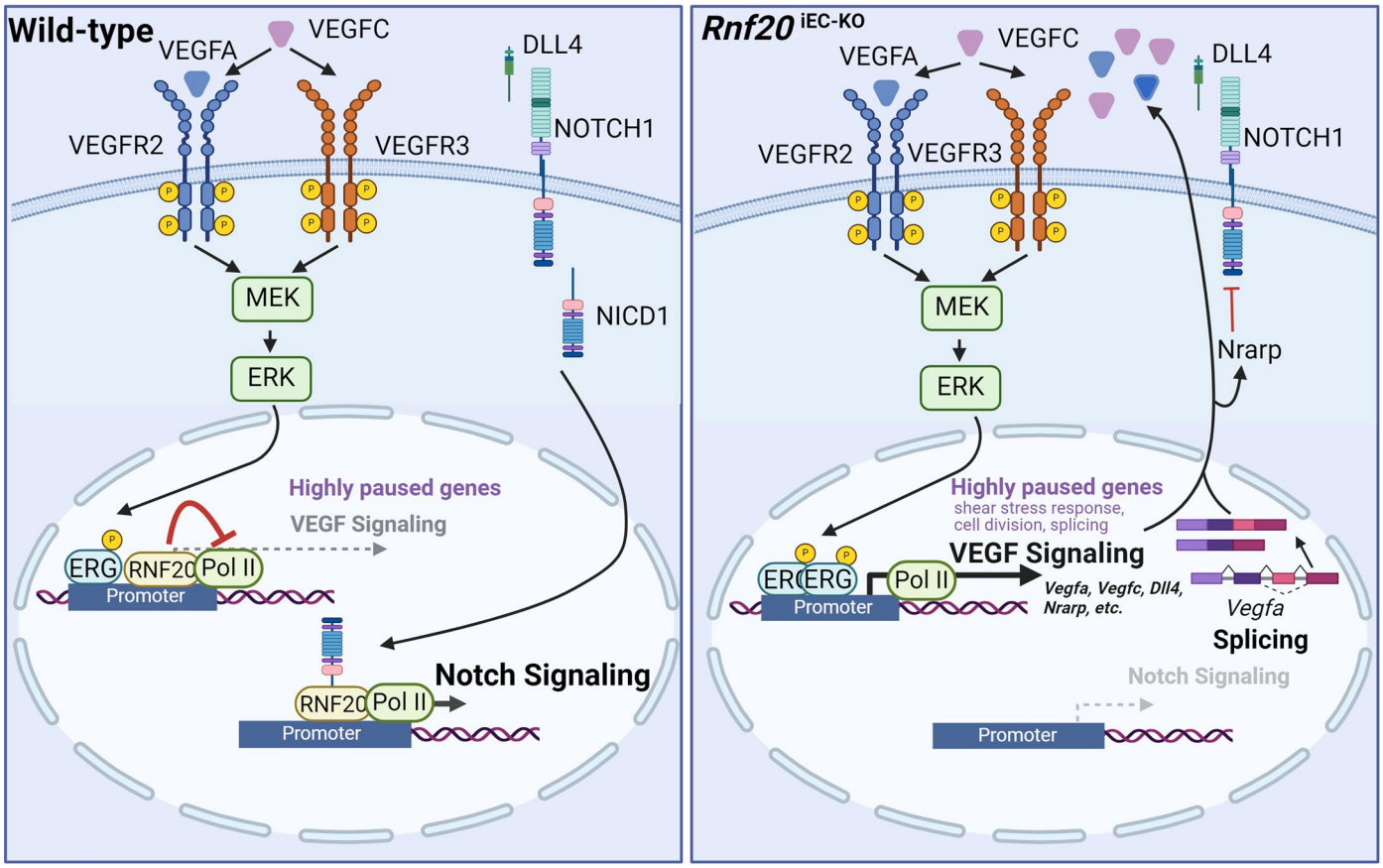

Extended Data Fig. 7 | Model. In wild-type retina endothelial cells, RNF20 promotes RNA Pol II pausing at highly paused genes involved in shear stress response, cell cycle regulation, mRNA splicing, and VEGFA signaling. Additionally, it interacts with N1ICD to regulate Notch-dependent transcriptional program by monoubiquitination of histone H2B. In retina ECs lacking RNF20 (*Rnf20*$^{iEC\text{-}KO}$), highly paused genes, including *Efnb2*, genes related to VEGFA signaling, as well as splicing regulators, are released for active elongation. This release is mediated, at least in part, by elevated ERG levels. Importantly, increased ERG levels can also induce Pol II pause release of highly paused genes by displacing RNF20 from chromatin. Further, RNF20 loss leads to widespread changes in splicing patterns, including splicing of VEGFA, resulting in an increase in the proteolytically stable VEGFA111 isoform. Exacerbated VEGF-VEGFR signaling and decreased Notch signaling, ultimately leads to uncontrolled specification of tip cells and compromised vessel growth upon RNF20 loss. The figure was designed with BioRender.

https://doi.org/10.1038/s44161-024-00546-5

Extended Data Table 1 | List of antibodies used in this study

Primary antibodies IF	Species	Clone	Company	Catalog #	Dilution
IB4-Alexa Fluor-488	Griffonia simplicifolia	-	Invitrogen	I21411	01:50
PECAM1 (CD31)	goat	polyclonal	R&D Systems	AF3628	1:200
PECAM1 (CD31) (390)	rat	monoclonal	eBioscience	17031180	1:100
ESM1	goat	polyclonal	R&D Systems	AF1999	1:100
ICAM2 (CD102) Clone 3C4(mIC2/4) (RUO)	rat	monoclonal	BD	553326	1:200
ERG (EPR3864)	rabbit	monoclonal	Abcam	ab92513	1:400
GOLPH4/GPP130	rabbit	polyclonal	Abcam	ab28049	1:200
DLL4	goat	polyclonal	R&D Systems	AF1389	1:100
VEGFR 3 (C28G5)	rabbit	monoclonal	Cell Signaling	2638S	1:100
VEGFA	goat	polyclonal	R&D Systems	AF493	1:100
VEGFC (E-6)	mouse	monoclonal	Santa Cruz Biotechnology	SC-374628	1:100

Secondary antibodies IF	Species	Clone	Company	Catalog #	Dilution
anti-Rabbit IgG (H+L) Alexa Fluor Plus 405	donkey		Thermo	A48258	1:200
anti-Rabbit IgG (H+L) Alexa Fluor 488	donkey		Thermo	A-21206	1:400
anti-Goat IgG (H+L) Alexa Fluor™ 555	donkey		Thermo	A-21432	1:400
anti-Mouse IgG (H+L) Alexa Fluor™ 555	donkey		Thermo	A-32773	1:400
anti-Rat IgG (H+L) Alexa Fluor™ 633	goat		Thermo	A-21094	1:400

Primary antibodies FACS	Species	Clone	Company	Catalog #	Dilution
Pecam1 (CD31) (Clone 390)-APC	Rat	monoclonal	eBioscience	17031180	0.5 µg/test

Primary antibodies WB	Species	Clone	Company	Catalog #	Dilution
RNF20 (D6E10)	rabbit	monoclonal	Cell Signalling	11974	1:1000
H2B	rabbit	polyclonal	Abcam	ab1790	1:2000
H2Bub1 (D11)	rabbit	monoclonal	Cell Signalling	5546	1:2000
NICD Cleaved Notch1 (Val1744) (D3B8)	rabbit	monoclonal	Cell Signalling	4147	1:1000
RBPSUH (D10A4)	rabbit	monoclonal	Cell Signalling	5313S	1:1000
TUBA1A clone B-5-1-2	mouse	monoclonal	Sigma	T5168	1:5000
DLL4 (D7N3H)	rabbit	monoclonal	Cell Signalling	96406	1:1000
ERG-1/2/3 (C-20)	rabbit	polyclonal	Santa Cruz Biotechnology	sc-353	1:1000
STAT3 (F-2)	mouse	monoclonal	Santa Cruz Biotechnology	sc-8079	1:1000
VEGFR 2 (55B11)	rabbit	monoclonal	Cell Signalling	2479	1:1000
Phospho-VEGFR 2 (Tyr1175) (19A10)	rabbit	monoclonal	Cell Signalling	2478	1:1000
VEGFR 3 (C28G5)	rabbit	monoclonal	Cell Signalling	2638	1:1000
AKT (pan) (11E7)	rabbit	monoclonal	Cell Signalling	4685	1:1000
Phospho-AKT (Ser473) (D9E)	rabbit	monoclonal	Cell Signalling	4060	1:1000
ERK1/2 (137F5)	rabbit	monoclonal	Cell Signalling	4695	1:1000
pERK1/2 (Thr202/Tyr204) (D13.14.4E)	rabbit	monoclonal	Cell Signalling	4370	1:1000
P38	rabbit	polyclonal	Cell Signalling	9212	1:1000
pP38 (Thr180/Tyr182) (D3F9)	rabbit	monoclonal	Cell Signalling	4511	1:1000
VE-Cadherin (D87F2)	rabbit	monoclonal	Cell Signalling	2500	1:1000

Antibodies used or ChIP	Species	Clone	Company	Catalog #	Dilution
H2Bub1 (D11)	rabbit	monoclonal	Cell Signalling	5546	0.5 µg/IP
Rpb1 NTD (total Pol II)	rabbit	monoclonal	Cell Signalling	14958S	1 µg/IP
NICD Cleaved Notch1 (Val1744) (D3B8)	rabbit	monoclonal	Cell Signalling	4147	1 µg/IP
ERG	rabbit	monoclonal	Abcam	ab92513	1 µg/IP

https://doi.org/10.1038/s44161-024-00546-5

Extended Data Table 2 | List of primer sequences used in this study

qPCR Primer

Primer name	seqeunce	species
Tuba1a_F	GAAGCAGCAACCATGCGTGA	
Tuba1a_R	CCTCCCCCAATGGTCTTGTC	Human
HPRT_F	GTCAAGGGCATATCCTACAACAA	
HPRT_R	AAGATGGTCAAGGTCGCAAG	Human
VEGFA_for	CCCACTGAGGAGTCCAACATC	
VEGFA111_rev2	CTCGGCTTGTCACATCTGCATTCA	Human
VEGFA_for	CCCACTGAGGAGTCCAACATC	
VEGFA111b_rev	cctggtgagagatctgcattcac	Human
VEGFA_for	CCCACTGAGGAGTCCAACATC	
VEGFA121_rev	TCGGCTTGTCACATTTTTCTTGT	Human
VEGFA_for	CCCACTGAGGAGTCCAACATC	
VEGFA121b_rev	cctggtgagagatttttcttgtcttgc	Human
VEGFA_for	CCCACTGAGGAGTCCAACATC	
VEGFA145_r3	TGTCACATACGCTCCAGGAC	Human
VEGFA165_for	AAGAAAATCCCTGTGGGCCTT	
VEGFA165a_rev	TTGTCACATCTGCAAGTACG	Human
VEGFA165_for	AAGAAAATCCCTGTGGGCCTT	
VEGFA165b_rev	TGGTGAGAGATCTGCAAGTACG	Human
VEGFA_for	CCCACTGAGGAGTCCAACATC	
VEGFA189_rev2	CACAGGGAACGCTCCAGGAC	Human
RNF20_F	cgggccttggaaaacga	
RNF20_R	aacagctgccttcttctcagg	Human
NOTCH3_F	GCCAAGCGGCTAAAGGTA	
NOTCH3_F	CACTGACGGCAATCCACA	Human
HES1_F	GTGTCAACACGACACCGGAT	
HES1_R	GGAATGCCGCGAGCTATCTT	Human
HES2_F	QIAGEN QuantiTect Primer Assays:	
HES2_R	QT01021475	Human
HEY1_F	TAATTGAGAAGCGCCGACGA	
HEY1_R	AGCTTAGCAGATCCTTGCTCC	Human
CCND1_F1	ggcggaggagaacaaacaga	
CCND1_R1	ggagggcggattggaaatga	Human
SOX17_for1	AGCAAGATGCTGGGCAAGTC	
SoOX17_rev1	TTGTAGTTGGGGTGGTCCTG	Human
ERG_F	GCCAGCACTATTAAGGAAGCC	
ERG_R	TGTCCATAGTCGCTGGAGGA	Human
STAT3_F	CTGCCGGAGAAACAGTTGG	
STAT3_R	AATCCAAGGGGCCAGAAACT	Human
FLT4_for1	CTCTGCCTGGGACTCCTGG	
FLT4-rev1	GATGACGTGTGACTCCTCCG	Human
DLL4_F	CCATGCAAGAATGGGGCAAC	
DLL4_R	GCCATCCTCCTGGTCCTTAC	Human
NRARP_F	CATTGAAATGGAGGCACAGA	
NRARP_R	ACCCACACACAGCTTCGATA	Human
VEGFA_for	CCCACTGAGGAGTCCAACATC	
total_VEGFA_rev	CTGCATTCACATTTGTTGTGCTG	Human
VEGFC_F1	TCTCTGTGGCGTGTTCTCTG	
VEGFC_R1	TCTTTGCTTGCATAAGCCGTG	Human
KDR_for1	AGACCGGCTGAAGCTAGGTA	
KDR_rev1	GAGCTCGATGCTCACTGTGT	Human

nature research

Corresponding author(s): Gergana Dobreva

Last updated by author(s): Aug 16, 2024

Reporting Summary

Nature Research wishes to improve the reproducibility of the work that we publish. This form provides structure for consistency and transparency in reporting. For further information on Nature Research policies, see our Editorial Policies and the Editorial Policy Checklist.

Statistics

For all statistical analyses, confirm that the following items are present in the figure legend, table legend, main text, or Methods section.

n/a	Confirmed	
☐	☒	The exact sample size (*n*) for each experimental group/condition, given as a discrete number and unit of measurement
☐	☒	A statement on whether measurements were taken from distinct samples or whether the same sample was measured repeatedly
☐	☒	The statistical test(s) used AND whether they are one- or two-sided *Only common tests should be described solely by name; describe more complex techniques in the Methods section.*
☒	☐	A description of all covariates tested
☐	☒	A description of any assumptions or corrections, such as tests of normality and adjustment for multiple comparisons
☐	☒	A full description of the statistical parameters including central tendency (e.g. means) or other basic estimates (e.g. regression coefficient) AND variation (e.g. standard deviation) or associated estimates of uncertainty (e.g. confidence intervals)
☐	☒	For null hypothesis testing, the test statistic (e.g. *F*, *t*, *r*) with confidence intervals, effect sizes, degrees of freedom and *P* value noted *Give P values as exact values whenever suitable.*
☒	☐	For Bayesian analysis, information on the choice of priors and Markov chain Monte Carlo settings
☒	☐	For hierarchical and complex designs, identification of the appropriate level for tests and full reporting of outcomes
☒	☐	Estimates of effect sizes (e.g. Cohen's *d*, Pearson's *r*), indicating how they were calculated

Our web collection on statistics for biologists contains articles on many of the points above.

Software and code

Policy information about availability of computer code

Data collection

The following standard software provided by instrument suppliers was used for data collection:
Histology: Zeiss Axio Scan (Zeiss)
Flow cytometry: BD FACS Aria IIu (BD Bioscience)
WB: Amersham Imager 600 (GE Healthcare Life Sciences)
Immunofluorescence : Leica DMi8 microscope (Leica); Zeiss LSM 710 confocal microscope(Zeiss)

Data analysis

IGV2.8.13, https://software.broadinstitute.org/software/igv/download
Image J 1.53, https://imagej.nih.gov/ij/download.html
BD FACSDiva Software (v.8.0.1, firmware version 1.49 BD FACSCanto II), https://www.bdbiosciences.com/en-eu/products/software/instrument-software/bd-facsdiva-software
Zen 2.3, https://www.zeiss.de/mikroskopie/produkte/mikroskopsoftware/zen-lite/zen-lite-download.html
Metascape version 3.5, https://metascape.org/gp/index.html#/main/step1
Heatmapper (d3Heatmap v.0.9.0), http://www.heatmapper.ca/expression/
GraphPad Prism 10, https://www.graphpad.com/
Venny 2.1, http://bioinformatics.psb.ugent.be/webtools/Venn/
STAR (v.2.7.3a), https://github.com/alexdobin/STAR/blob/master/doc/STARmanual.pdf
Trimmomatic (v.0.39), http://www.usadellab.org/cms/?page=trimmomatic
Homer (v.4.11.1), http://homer.ucsd.edu/homer/data/software/
EdgeR (v.3.42.4), https://bioconductor.org/packages/release/bioc/html/edgeR.html
BamTools (v.2.5.1), https://github.com/pezmaster31/bamtools
MultiQC (v.1.14), https://multiqc.info/
DESeq2 (v.1.40.0) http://bioconductor.org/packages/release/bioc/vignettes/DESeq2/inst/doc/DESeq2.html
Ngsplot (v.2.41.4), http://github.com/shenlab-sinai/ngsplot
Homer (v.3.12), http://homer.ucsd.edu/homer/motif/

Bowtie2 (v.2.4.4) , https://github.com/BenLangmead/bowtie2
SAMtools (v.1.7), http://www.htslib.org/
Picard-tools (v.1.119), https://broadinstitute.github.io/picard/
deepTools (v.3.5.1), https://deeptools.readthedocs.io/en/develop/
MACS2 (v.2.2.7.1), https://pypi.org/project/MACS2/
R package DiffBind (v.3.4.11), http://bioconductor.org/packages/release/bioc/vignettes/DiffBind/inst/doc/DiffBind.pdf
R package rstatix (v.0.7.2), https://cran.r-project.org/web/packages/rstatix/index.html
R package EnhancedVolcano (v.1.18.0), https://github.com/kevinblighe/EnhancedVolcano
DEXSeq R-package (v.1.40.0), https://bioconductor.org/packages/release/bioc/vignettes/DEXSeq/inst/doc/DEXSeq.html
ATAC-seq pipline, https://github.com/ENCODE-DCC/atac-seq-pipeline
TOBIAS footprinting package (v.0.14.0)
Cytoscape (v.3.6.1), https://github.com/cytoscape/cytoscape/releases/3.6.1/
Seurat (v4.1.0), https://satijalab.org/seurat/

For manuscripts utilizing custom algorithms or software that are central to the research but not yet described in published literature, software must be made available to editors and reviewers. We strongly encourage code deposition in a community repository (e.g. GitHub). See the Nature Research guidelines for submitting code & software for further information.

Data

Policy information about availability of data

All manuscripts must include a data availability statement. This statement should provide the following information, where applicable:

- Accession codes, unique identifiers, or web links for publicly available datasets
- A list of figures that have associated raw data
- A description of any restrictions on data availability

Sequencing data generated in this study have been deposited in GEO (accession number GSE212524). Processed data are included in the Source Data for each figure. Single-cell data from neonatal mouse retinas (GSE175895), ChIP-seq of ERG (GSE124893) and ETS1 (GSM2442778) in HUVECs were retrieved from previously published studies. Figures that have associated raw data: Fig. 3a-d, Fig 3f-k, Fig. 4a-c, Fig. 4f, Fig. 5h, i and k, Fig. 6a-g, Extended Data Fig. 2a-g, 2i and 2J, Extended Data Fig. 3a-b, Extended Data Fig. 4a-d, 4g and h, Extended Data Fig. 5a-c.

Field-specific reporting

Please select the one below that is the best fit for your research. If you are not sure, read the appropriate sections before making your selection.

☒ Life sciences ☐ Behavioural & social sciences ☐ Ecological, evolutionary & environmental sciences

For a reference copy of the document with all sections, see nature.com/documents/nr-reporting-summary-flat.pdf

Life sciences study design

All studies must disclose on these points even when the disclosure is negative.

Sample size	No statistical measures were used to determine sample size. Sample size is based on our experience and on publications by other groups for example Pontes-Quero et al. (2019) and Kalna et al. (2019).
Data exclusions	None.
Replication	All experiments were performed at least three independent times. All attempts at replication were successful.
Randomization	No statistical methods were used for randomization. For experiments involving mice, genotypes were determined after tamoxifen injection, and the mice were then separated into control and mutant groups for statistical analysis. For in vitro experiments the experimental design inherently controlled for variation. This was achieved by using technical replicates, standardizing experimental conditions, and ensuring that the same samples were subjected to different conditions. As such, random allocation was not necessary for these specific experiments.
Blinding	The investigators were not blinded in regard to allocation of samples during experiments and outcome assessment. However, the outcomes were quantitative and not subjective.

Reporting for specific materials, systems and methods

We require information from authors about some types of materials, experimental systems and methods used in many studies. Here, indicate whether each material, system or method listed is relevant to your study. If you are not sure if a list item applies to your research, read the appropriate section before selecting a response.

Materials & experimental systems

n/a	Involved in the study
☐	☒ Antibodies
☐	☒ Eukaryotic cell lines
☒	☐ Palaeontology and archaeology
☐	☒ Animals and other organisms
☒	☐ Human research participants
☒	☐ Clinical data
☒	☐ Dual use research of concern

Methods

n/a	Involved in the study
☐	☒ ChIP-seq
☐	☒ Flow cytometry
☒	☐ MRI-based neuroimaging

Antibodies

Antibodies used

Primary antibodies IF, Species, Clone, Company, Catalog #, Dilution
IB4-Alexa Fluor-488, Griffonia simplicifolia, - , Invitrogen, I21411, 01:50
PECAM1 (CD31), goat, polyclonal, R&D Systems, AF3628, 1:200
PECAM1 (CD31) (390), rat , monoclonal, eBioscience, 17031180, 1:100
ESM1, goat, polyclonal, R&D Systems, AF1999, 1:100
ICAM2 (CD102) Clone 3C4(mIC2/4) (RUO), rat, monoclonal, BD, 553326, 1:200
ERG (EPR3864), rabbit, monoclonal, Abcam, ab92513, 1:400
GOLPH4/GPP130, rabbit, polyclonal, Abcam, ab28049, 1:200
DLL4, goat, polyclonal, R&D Systems, AF1389, 1:100
VEGFR 3 (C28G5), rabbit , monoclonal, Cell Signaling, 2638S, 1:100
VEGFA, goat, polyclonal, R&D Systems, AF493, 1:100
VEGFC (E-6), mouse, monoclonal, Santa Cruz Biotechnology, SC-374628, 1:100

Secondary antibodies IF, Species, Clone, Company, Catalog #, Dilution
anti-Rabbit IgG (H+L) Alexa Fluor Plus 405, donkey, , Thermo, A48258, 1:200
anti-Rabbit IgG (H+L) Alexa Fluor 488 , donkey, , Thermo, A-21206 , 1:400
anti-Goat IgG (H+L) Alexa Fluor™ 555, donkey, , Thermo, A-21432, 1:400
anti-Mouse IgG (H+L) Alexa Fluor™ 555, donkey, , Thermo, A-32773, 1:400
anti-Rat IgG (H+L) Alexa Fluor™ 633, goat, , Thermo, A-21094, 1:400

Primary antibodies FACS, Species, Clone, Company, Catalog #, Dilution
Pecam1 (CD31) (Clone 390)-APC, Rat , monoclonal, eBioscience, 17031180, 0.5 µg/test

Primary antibodies WB, Species, Clone, Company, Catalog #, Dilution
RNF20 (D6E10), rabbit, monoclonal, Cell Signalling, 11974, 1:1000
H2B, rabbit, polyclonal, Abcam, ab1790, 1:2000
H2Bub1 (D11), rabbit, monoclonal, Cell Signalling, 5546, 1:2000
NICD Cleaved Notch1 (Val1744) (D3B8) , rabbit, monoclonal, Cell Signalling, 4147, 1:1000
RBPSUH (D10A4), rabbit, monoclonal, Cell Signalling, 5313S, 1:1000
TUBA1A clone B-5-1-2, mouse, monoclonal, Sigma, T5168, 1:5000
DLL4 (D7N3H), rabbit, monoclonal, Cell Signalling, 96406, 1:1000
ERG-1/2/3 (C-20), rabbit, polyclonal, Santa Cruz Biotechnology, sc-353, 1:1000
STAT3 (F-2), mouse, monoclonal, Santa Cruz Biotechnology, sc-8079, 1:1000
VEGFR 2 (55B11) , rabbit, monoclonal, Cell Signalling, 2479, 1:1000
Phospho-VEGFR 2 (Tyr1175) (19A10), rabbit, monoclonal, Cell Signalling, 2478, 1:1000
VEGFR 3 (C28G5), rabbit, monoclonal, Cell Signalling, 2638, 1:1000
AKT (pan) (11E7), rabbit, monoclonal, Cell Signalling, 4685, 1:1000
Phospho-AKT (Ser473) (D9E), rabbit, monoclonal, Cell Signalling, 4060, 1:1000
ERK1/2 (137F5), rabbit, monoclonal, Cell Signalling, 4695, 1:1000
pERK1/2 (Thr202/Tyr204) (D13.14.4E), rabbit, monoclonal, Cell Signalling, 4370, 1:1000
P38 , rabbit, polyclonal, Cell Signalling, 9212, 1:1000
pP38 (Thr180/Tyr182) (D3F9), rabbit, monoclonal, Cell Signalling, 4511, 1:1000
VE-Cadherin (D87F2), rabbit, monoclonal, Cell Signalling, 2500, 1:1000

Antibodies used or ChIP, Species, Clone, Company, Catalog #, Dilution
H2Bub1 (D11), rabbit, monoclonal, Cell Signalling, 5546, 0.5 µg/IP
Rpb1 NTD (total Pol II), rabbit, monoclonal, Cell Signalling, 14958S, 1 µg/IP
NICD Cleaved Notch1 (Val1744) (D3B8) , rabbit, monoclonal, Cell Signalling, 4147, 1 µg/IP
ERG, rabbit, monoclonal, Abcam, ab92513, 1 µg/IP

Validation

All antibodies used were purchased from commercial vendors and were selected because they have been validated by the manufacturer and in different publications. Validation details and relevant publications are detailed on their respective websites.

Eukaryotic cell lines

Policy information about cell lines

Cell line source(s)	HUVECs from pooled donors were purchased from Lonza (#CC-2519) or PromoCell (#C-12208) and cultured in complete EGM-MV2 medium (#C-22022, PromoCell) supplemented with 1x penicillin/streptomycin. Human embryonic kidney cells (HEK293T) were purchased from Life Technologies (#R70007, Thermo Fisher Scientific) and cultured in DMEM high glucose GlutaMAX (#61965059, Gibco) supplemented with 10% FBS 1x penicillin/streptomycin and 1x sodium pyruvate..
Authentication	HEK293T cells were authenticated by ATCC (STR profiling), while HUVECs by Lonza and PromoCell (CD31/105+; PCR, Phenotypic characterization, fuctional assay, mycoplasma testing).
Mycoplasma contamination	Cell lines were mycoplasma negative.
Commonly misidentified lines (See ICLAC register)	No commonly misidentified lines were used in the study.

Animals and other organisms

Policy information about studies involving animals; ARRIVE guidelines recommended for reporting animal research

Laboratory animals	The Rnf20tm1a(EUCOMM)Wtsi line was generated by microinjection of Rnf20 tm1a(EUCOMM)Wtsi ES cells, obtained from the European Conditional Mouse Mutagenesis Program (EUCOMM), into blastocysts (Extended Data Fig. 1a). For the generation of a conditional (floxed) allele Rnf20tm1c(EUCOMM)Wtsi line, the Rnf20tm1a(EUCOMM)Wtsi mouse line was crossed with germline FLP deleter mouse line. To induce endothelial restricted deletion, the resulting Rnf20 Rnf20tm1c(EUCOMM)Wtsi mice carrying a conditional floxed allele, were bred to a line carrying the tamoxifen-inducible recombinase CreERT2 driven by the platelet derived growth factor subunit B (Pdgfb) promoter, i.e. Pdgfb-iCreERT218. To activate CreERT2, pups were administered 25µl of 3mg/ml 4-hydroxytamoxifen (4OHT, #H7904, Sigma) intraperitoneally from P1 to P4. Retinas were harvested between P6 and P28. All animal experiments were performed according to the regulations issued by the Committee for Animal Rights Protection of the State of Baden-Württemberg (Regierungspraesidium Karlsruhe, Experimental protocol Az.: 35-9185.81/G-181/17). For the experiments described in the manuscript, we used mice at P7, P14, P21 or P28. Breeding pairs were crossed when they were older than 2 months. The mice were housed in sealed, individually ventilated cages (IVCs) within a controlled environment with a 12-hour dark/light cycle (lights on at 7:00 AM and off at 7:00 PM). The ambient temperature was maintained at 22 ± 2°C, and the relative humidity was kept at 50 ± 10%. All mice had ad libitum access to food and water, and were provided with appropriate bedding and environmental enrichment within the sealed cages. Breeding pairs were crossed when they were older than 2 months.
Wild animals	No wild animals were used in this study.
Field-collected samples	No field-collected samples were used in this study.
Ethics oversight	All animal experiments were performed according to the regulations issued by the Committee for Animal Rights Protection of the State of Baden-Württemberg (Regierungspraesidium Karlsruhe, Experimental protocol Az.: 35-9185.81/G-181/17).

Note that full information on the approval of the study protocol must also be provided in the manuscript.

ChIP-seq

Data deposition

☒ Confirm that both raw and final processed data have been deposited in a public database such as GEO.

☒ Confirm that you have deposited or provided access to graph files (e.g. BED files) for the called peaks.

Data access links *May remain private before publication.*	NGS data are publicly available in GEO (accession number GSE212524).
Files in database submission	GSM6533907 P7-Retinal-EC-Rnf20-Ctrl-RNAseq-Rep1 GSM6533908 P7-Retinal-EC-Rnf20-Ctrl-RNAseq-Rep2 GSM6533909 P7-Retinal-EC-Rnf20-Ctrl-RNAseq-Rep3 GSM6533910 P7-Retinal-EC-Rnf20-KO-RNAseq-Rep1 GSM6533911 P7-Retinal-EC-Rnf20-KO-RNAseq-Rep2 GSM6533912 P7-Retinal-EC-Rnf20-KO-RNAseq-Rep3 GSM6533947 01HUVEC-siCtr1-60h GSM6533948 01HUVEC-siCtr2-60h GSM6533949 01HUVEC-siCtr3-60h GSM6533950 01HUVEC-siRNF20-1-60h GSM6533951 01HUVEC-siRNF20-2-60h GSM6533952 01HUVEC-siRNF20-3-60h GSM6533953 P7-Retina-EC-ATACseq-CTR-rep1 GSM6533954 P7-Retina-EC-ATACseq-KO-rep2 GSM6533955 P7-Retina-EC-ATACseq-CTR-rep2 GSM6533956 P7-Retina-EC-ATACseq-KO-rep1

GSM7060764 03HUVEC_POL2_IP_siCTR_rep1
GSM7060765 03HUVEC_POL2_IP_siCTR_rep2
GSM7060766 03HUVEC_POL2_IP_siCTR_rep3
GSM7060767 04HUVEC_POL2_IP_siRNF20_rep1
GSM7060768 04HUVEC_POL2_IP_siRNF20_rep2
GSM7060769 04HUVEC_POL2_IP_siRNF20_rep3
GSM7060770 05HUVEC_INPUT_siCTR_rep1
GSM7060771 05HUVEC_INPUT_siCTR_rep2
GSM7060772 05HUVEC_INPUT_siCTR_rep3
GSM7060773 06HUVEC_INPUT_siRNF20_rep1
GSM7060774 06HUVEC_INPUT_siRNF20_rep2
GSM7060775 06HUVEC_INPUT_siRNF20_rep3
GSM7877381 H2Bub_IP_siCTR_HUVEC_r1_ChIP_seq
GSM7877382 H2Bub_IP_siCTR_HUVEC_r2_ChIP_seq
GSM7877383 H2Bub_IP_siCTR_HUVEC_r3_ChIP_seq
GSM7877384 H2Bub_IP_siRNF20_HUVEC_r1_ChIP_seq
GSM7877385 H2Bub_IP_siRNF20_HUVEC_r2_ChIP_seq
GSM7877386 H2Bub_IP_siRNF20_HUVEC_r3_ChIP_seq
GSM7877387 HUVEC_siCTR_60h_ATAC_r1
GSM7877388 HUVEC_siCTR_60h_ATAC_r2
GSM7877389 HUVEC_siCTR_60h_ATAC_r3
GSM7877390 HUVEC_siCTR_60h_ATAC_r4
GSM7877391 HUVEC_siRN20_60h_ATAC_r1
GSM7877392 HUVEC_siRN20_60h_ATAC_r2
GSM7877393 HUVEC_siRN20_60h_ATAC_r3
GSM7877394 HUVEC_siRN20_60h_ATAC_r4
GSM8291882 HUV_PLKO_Ctr_P2t_IP_ChiP_r1
GSM8291883 HUV_PLKO_Ctr_P2t_IP_ChiP_r2
GSM8291884 HUV_ERG_OE_P2t_IP_ChiP_r1
GSM8291885 HUV_ERG_OE_P2t_IP_ChiP_r2
GSM8291886 HUV_PLKO_Ctr_Inp_r1
GSM8291887 HUV_PLKO_Ctr_Inp_r2
GSM8291888 HUV_ERG_OE_Inp_r1
GSM8291889 HUV_ERG_OE_Inp_r2

Genome browser session
(e.g. UCSC)

Methodology

Replicates: "n" number indicated in the figure legends represents RNA-Seq and ChIP-Seq experiments from independent biological replicates.

Sequencing depth:
HUVEC ATAC seq: 24 000 000 reads
Retina EC ATAC seq: 31 000 000 - 40 000 000 reads paired-end
Pol II ChIP seq from control and siRNF20 transfected HUVECs: 20 000 000 INPUT; 30 000 000 IP
Pol II ChIP from control and ERG overexpressing HUVECs: 27 000 000 – 50 000 000 INPUT; 37 000 000 - 69 000 000 IP reads
H2Bub ChIP seq from control and siRNF20 transfected HUVECs: 73 000 000 – 80 000 000 paired end

Antibodies: RNA Polymerase II ChIP-Seq, Cell Signalling, Cat N 14958S; H2Bub1, Cell Signalling, 5546

Peak calling parameters: MACS14 (default settings)

Data quality: FastQC

Software: As listed in the Data analysis section.

Flow Cytometry

Plots

Confirm that:

☒ The axis labels state the marker and fluorochrome used (e.g. CD4-FITC).

☒ The axis scales are clearly visible. Include numbers along axes only for bottom left plot of group (a 'group' is an analysis of identical markers).

☐ All plots are contour plots with outliers or pseudocolor plots.

☐ A numerical value for number of cells or percentage (with statistics) is provided.

Methodology

Sample preparation	P7 retinas were dissected and digested with a collagenase enzyme solution (1mg/ml collagenase I (#LS004196, Worthington), 0.1 mg/ml DNAse I (#10104159001, Merck) in HBSS) for 1h at 37°C followed by filtering the cell suspension through a 70 µm cell strainer with basal medium (DMEM high glucose, 20% FBS, 1x penicillin/streptomycin, 1x l-glutamin, 25 mM HEPES). After centrifugation and washing, cells were stained with a CD31-APC coupled antibody for 30 min and sorted with BD FACS Aria IIu (BD Bioscience) for living, CD31+ cells.
Instrument	BD FACSCanto II, BD FACSAria IIu
Software	Data were collected and analyzed using BD FACSDivaTM software(version8.0.1).
Cell population abundance	Post sorting confirmed the high purity of the sorted populations.
Gating strategy	Unstained cells were used to define negative cell populations and set gates for analysis.

☐ Tick this box to confirm that a figure exemplifying the gating strategy is provided in the Supplementary Information.